# Appendix B

# Number of gammas in $^{nat}$Xe

| Xenon isotope | Gamma energy (keV) | From level (keV) | To level (keV) | $I_\gamma$ per 100 captures | Xenon isotope | Gamma energy (keV) | From level (keV) | To level (keV) | $I_\gamma$ per 100 captures |
|---|---|---|---|---|---|---|---|---|---|
| $^{132}$Xe | 667.72 | 667.72 | 0.0 | 64.73 | $^{125}$Xe | 644.56 | 1441.2 | 796.62 | 2.876 |
| $^{132}$Xe | 6466.1 | 8935.2 | 2469.1 | 24.07 | $^{132}$Xe | 5059.9 | 8935.2 | 3875.3 | 2.808 |
| $^{132}$Xe | 772.61 | 1440.3 | 667.72 | 22.55 | $^{132}$Xe | 4908.2 | 8935.2 | 4027.0 | 2.588 |
| $^{130}$Xe | 536.09 | 536.09 | 0.0 | 16.60 | $^{125}$Xe | 774.54 | 2215.7 | 1441.2 | 2.445 |
| $^{132}$Xe | 1317.9 | 1985.7 | 667.72 | 15.88 | $^{132}$Xe | 1397.4 | 3792.3 | 2394.9 | 2.341 |
| $^{132}$Xe | 6379.8 | 8935.2 | 2555.4 | 10.66 | $^{130}$Xe | 702.80 | 6290.5 | 5587.7 | 2.275 |
| $^{130}$Xe | 668.52 | 1204.6 | 536.09 | 10.25 | $^{130}$Xe | 2965.3 | 9255.8 | 6290.5 | 2.275 |
| $^{132}$Xe | 483.46 | 2469.1 | 1985.7 | 9.824 | $^{130}$Xe | 466.39 | 2841.6 | 2375.2 | 2.269 |
| $^{132}$Xe | 600.03 | 2040.4 | 1440.3 | 8.355 | $^{132}$Xe | 1120.9 | 3875.3 | 2754.4 | 2.247 |
| $^{132}$Xe | 5754.4 | 8935.2 | 3180.8 | 7.847 | $^{132}$Xe | 1858.2 | 4027.0 | 2168.8 | 2.194 |
| $^{132}$Xe | 569.75 | 2555.4 | 1985.7 | 7.196 | $^{132}$Xe | 954.58 | 2394.9 | 1440.3 | 2.177 |
| $^{132}$Xe | 1028.8 | 2469.1 | 1440.3 | 6.778 | $^{132}$Xe | 522.67 | 1963.0 | 1440.3 | 1.988 |
| $^{132}$Xe | 1887.7 | 2555.4 | 667.72 | 6.404 | $^{132}$Xe | 2168.8 | 2168.8 | 0.0 | 1.972 |
| $^{125}$Xe | 111.78 | 111.78 | 0.0 | 6.344 | $^{125}$Xe | 884.18 | 3099.9 | 2215.7 | 1.911 |
| $^{132}$Xe | 1140.4 | 3180.8 | 2040.4 | 6.278 | $^{130}$Xe | 696.28 | 3071.5 | 2375.2 | 1.911 |
| $^{130}$Xe | 739.48 | 1944.1 | 1204.6 | 5.859 | $^{132}$Xe | 1501.1 | 2168.8 | 667.72 | 1.775 |
| $^{132}$Xe | 5142.9 | 8935.2 | 3792.3 | 5.783 | $^{132}$Xe | 5691.8 | 8935.2 | 3243.4 | 1.707 |
| $^{132}$Xe | 1801.4 | 2469.1 | 667.72 | 5.501 | $^{125}$Xe | 971.00 | 4070.9 | 3099.9 | 1.639 |
| $^{130}$Xe | 752.79 | 2696.9 | 1944.1 | 5.344 | $^{132}$Xe | 1985.7 | 1985.7 | 0.0 | 1.588 |
| $^{130}$Xe | 275.45 | 2972.3 | 2696.9 | 5.225 | $^{132}$Xe | 1740.5 | 3180.8 | 1440.3 | 1.569 |
| $^{130}$Xe | 720.84 | 3693.2 | 2972.3 | 4.921 | $^{130}$Xe | 804.89 | 4347.1 | 3542.2 | 1.543 |
| $^{125}$Xe | 140.82 | 252.60 | 111.78 | 4.608 | $^{125}$Xe | 184.08 | 295.86 | 111.78 | 1.512 |
| $^{132}$Xe | 630.20 | 1297.9 | 667.72 | 4.384 | $^{130}$Xe | 949.60 | 5296.7 | 4347.1 | 1.494 |
| $^{132}$Xe | 8267.5 | 8935.2 | 667.72 | 4.323 | $^{130}$Xe | 3959.1 | 9255.8 | 5296.7 | 1.494 |
| $^{132}$Xe | 5235.7 | 8935.2 | 3699.5 | 4.186 | $^{130}$Xe | 821.87 | 3893.4 | 3071.5 | 1.442 |
| $^{130}$Xe | 854.99 | 2059.6 | 1204.6 | 3.992 | $^{132}$Xe | 5877.0 | 8935.2 | 3058.1 | 1.432 |
| $^{125}$Xe | 57.940 | 310.54 | 252.60 | 3.917 | $^{130}$Xe | 3651.0 | 9255.8 | 5604.8 | 1.407 |
| $^{130}$Xe | 315.60 | 2375.2 | 2059.6 | 3.666 | $^{130}$Xe | 5956.8 | 9255.8 | 3299.0 | 1.375 |
| $^{132}$Xe | 1236.9 | 3792.3 | 2555.4 | 3.442 | $^{132}$Xe | 505.80 | 1803.7 | 1297.9 | 1.369 |
| $^{125}$Xe | 486.08 | 796.62 | 310.54 | 3.226 | $^{130}$Xe | 700.62 | 3542.2 | 2841.6 | 1.368 |

continues on next page

Table B.1: Number of gammas per 100 thermal neutron captures in $^{nat}$Xe

continued from previous page

| Xenon isotope | Gamma energy (keV) | From level (keV) | To level (keV) | $I_\gamma$ per 100 captures | Xenon isotope | Gamma energy (keV) | From level (keV) | To level (keV) | $I_\gamma$ per 100 captures |
|---|---|---|---|---|---|---|---|---|---|
| $^{130}$Xe | 997.20 | 5587.7 | 4590.5 | 3.207 | $^{132}$Xe | 1280.4 | 3243.4 | 1963.0 | 1.366 |
| $^{130}$Xe | 897.33 | 4590.5 | 3693.2 | 3.207 | $^{132}$Xe | 1895.8 | 3699.5 | 1803.7 | 1.273 |
| $^{132}$Xe | 4840.7 | 8935.2 | 4094.5 | 2.946 | $^{132}$Xe | 2086.7 | 2754.4 | 667.72 | 1.248 |
| $^{132}$Xe | 3699.5 | 3699.5 | 0.0 | 2.913 | $^{132}$Xe | 4981.0 | 8935.2 | 3954.2 | 1.239 |
| $^{130}$Xe | 586.06 | 1122.1 | 536.09 | 2.908 | $^{125}$Xe | 3532.4 | 7603.3 | 4070.9 | 1.238 |
| $^{130}$Xe | 941.93 | 4635.1 | 3693.2 | 1.230 | $^{131}$Xe | 606.73 | 971.22 | 364.49 | 0.6350 |
| $^{130}$Xe | 925.80 | 5560.9 | 4635.1 | 1.230 | $^{130}$Xe | 246.98 | 2633.2 | 2386.2 | 0.6104 |
| $^{130}$Xe | 3364.1 | 9255.8 | 5891.7 | 1.230 | $^{130}$Xe | 595.50 | 4942.6 | 4347.1 | 0.5960 |
| $^{130}$Xe | 330.80 | 5891.7 | 5560.9 | 1.230 | $^{131}$Xe | 364.49 | 364.49 | 0.0 | 0.5909 |
| $^{125}$Xe | 300.90 | 596.76 | 295.86 | 1.151 | $^{132}$Xe | 2577.4 | 3875.3 | 1297.9 | 0.5617 |
| $^{130}$Xe | 229.89 | 3071.5 | 2841.6 | 1.127 | $^{132}$Xe | 2796.6 | 4094.5 | 1297.9 | 0.5556 |
| $^{132}$Xe | 1171.2 | 2469.1 | 1297.9 | 1.120 | $^{130}$Xe | 646.75 | 4540.1 | 3893.4 | 0.5514 |
| $^{130}$Xe | 2762.6 | 2762.6 | 0.0 | 1.105 | $^{130}$Xe | 2978.5 | 2978.5 | 0.0 | 0.5482 |
| $^{132}$Xe | 1115.1 | 2555.4 | 1440.3 | 1.029 | $^{125}$Xe | 736.03 | 2272.2 | 1536.2 | 0.5460 |
| $^{125}$Xe | 715.40 | 1925.3 | 1209.9 | 0.9781 | $^{125}$Xe | 574.74 | 870.60 | 295.86 | 0.5405 |
| $^{132}$Xe | 6220.8 | 8935.2 | 2714.4 | 0.9639 | $^{132}$Xe | 1539.1 | 4094.5 | 2555.4 | 0.5303 |
| $^{130}$Xe | 6369.8 | 9255.8 | 2886.0 | 0.9406 | $^{125}$Xe | 665.60 | 1536.2 | 870.60 | 0.5278 |
| $^{130}$Xe | 6301.5 | 9255.8 | 2954.3 | 0.9406 | $^{132}$Xe | 2390.4 | 3058.1 | 667.72 | 0.5242 |
| $^{125}$Xe | 778.83 | 2704.1 | 1925.3 | 0.9340 | $^{132}$Xe | 6748.0 | 8935.2 | 2187.2 | 0.5232 |
| $^{125}$Xe | 613.15 | 1209.9 | 596.76 | 0.9327 | $^{130}$Xe | 2653.0 | 3189.1 | 536.09 | 0.5222 |
| $^{130}$Xe | 2649.9 | 9255.8 | 6605.9 | 0.9320 | $^{130}$Xe | 5713.6 | 9255.8 | 3542.2 | 0.5217 |
| $^{130}$Xe | 1018.2 | 6605.9 | 5587.7 | 0.9320 | $^{130}$Xe | 431.11 | 2375.2 | 1944.1 | 0.5132 |
| $^{130}$Xe | 2176.9 | 3299.0 | 1122.1 | 0.9135 | $^{130}$Xe | 6622.6 | 9255.8 | 2633.2 | 0.5066 |
| $^{130}$Xe | 191.70 | 2954.3 | 2762.6 | 0.8877 | $^{132}$Xe | 6949.5 | 8935.2 | 1985.7 | 0.4957 |
| $^{130}$Xe | 470.73 | 3542.2 | 3071.5 | 0.8620 | $^{132}$Xe | 791.44 | 2754.4 | 1963.0 | 0.4743 |
| $^{132}$Xe | 1785.4 | 3954.2 | 2168.8 | 0.8545 | $^{130}$Xe | 1763.9 | 2886.0 | 1122.1 | 0.4739 |
| $^{132}$Xe | 2054.1 | 4094.5 | 2040.4 | 0.8418 | $^{130}$Xe | 6066.7 | 9255.8 | 3189.1 | 0.4703 |
| $^{132}$Xe | 1136.0 | 1803.7 | 667.72 | 0.8353 | $^{130}$Xe | 1264.1 | 2386.2 | 1122.1 | 0.4703 |
| $^{132}$Xe | 428.75 | 2469.1 | 2040.4 | 0.8056 | $^{125}$Xe | 4899.2 | 7603.3 | 2704.1 | 0.4696 |
| $^{130}$Xe | 6277.3 | 9255.8 | 2978.5 | 0.7960 | $^{130}$Xe | 5849.7 | 9255.8 | 3406.1 | 0.4560 |

continues on next page

Table B.4: Number of gammas per 100 thermal neutron captures in $^{nat}$Xe

continued from previous page

| Xenon isotope | Gamma energy (keV) | From level (keV) | To level (keV) | $I_\gamma$ per 100 captures | Xenon isotope | Gamma energy (keV) | From level (keV) | To level (keV) | $I_\gamma$ per 100 captures |
|---|---|---|---|---|---|---|---|---|---|
| $^{130}$Xe | 453.75 | 4347.1 | 3893.4 | 0.7713 | $^{130}$Xe | 1122.1 | 1122.1 | 0.0 | 0.4478 |
| $^{132}$Xe | 2714.4 | 2714.4 | 0.0 | 0.7472 | $^{132}$Xe | 388.13 | 3058.1 | 2670.0 | 0.4194 |
| $^{130}$Xe | 6184.3 | 9255.8 | 3071.5 | 0.7235 | $^{130}$Xe | 8133.7 | 9255.8 | 1122.1 | 0.4124 |
| $^{130}$Xe | 5720.6 | 9255.8 | 3535.2 | 0.7235 | $^{125}$Xe | 5387.6 | 7603.3 | 2215.7 | 0.4124 |
| $^{130}$Xe | 662.20 | 5604.8 | 4942.6 | 0.7033 | $^{125}$Xe | 782.96 | 3487.1 | 2704.1 | 0.4064 |
| $^{130}$Xe | 633.20 | 5604.8 | 4971.6 | 0.7033 | $^{125}$Xe | 4116.2 | 7603.3 | 3487.1 | 0.4064 |
| $^{130}$Xe | 431.50 | 4971.6 | 4540.1 | 0.7033 | $^{132}$Xe | 1519.5 | 2187.2 | 667.72 | 0.3994 |
| $^{132}$Xe | 1925.7 | 4094.5 | 2168.8 | 0.6987 | $^{131}$Xe | 683.00 | 1654.2 | 971.22 | 0.3980 |
| $^{125}$Xe | 4392.5 | 7603.3 | 3210.8 | 0.6960 | $^{131}$Xe | 4950.9 | 6605.1 | 1654.2 | 0.3980 |
| $^{130}$Xe | 1687.4 | 2223.5 | 536.09 | 0.6544 | $^{125}$Xe | 426.31 | 736.85 | 310.54 | 0.3953 |
| $^{132}$Xe | 1986.6 | 4027.0 | 2040.4 | 0.3948 | $^{130}$Xe | 841.87 | 3814.2 | 2972.3 | 0.2649 |
| $^{130}$Xe | 1850.1 | 2386.2 | 536.09 | 0.3904 | $^{130}$Xe | 5441.6 | 9255.8 | 3814.2 | 0.2649 |
| $^{129}$Xe | 39.578 | 39.578 | 0.0 | 0.3884 | $^{130}$Xe | 510.38 | 1632.5 | 1122.1 | 0.2646 |
| $^{132}$Xe | 2150.5 | 3954.2 | 1803.7 | 0.3845 | $^{125}$Xe | 5458.8 | 7603.3 | 2144.5 | 0.2612 |
| $^{130}$Xe | 1311.7 | 3535.2 | 2223.5 | 0.3720 | $^{125}$Xe | 1547.7 | 2144.5 | 596.76 | 0.2612 |
| $^{130}$Xe | 894.94 | 2017.1 | 1122.1 | 0.3686 | $^{130}$Xe | 846.93 | 4540.1 | 3693.2 | 0.2592 |
| $^{125}$Xe | 954.50 | 4573.5 | 3619.0 | 0.3673 | $^{125}$Xe | 5301.8 | 7603.3 | 2301.5 | 0.2578 |
| $^{125}$Xe | 3029.8 | 7603.3 | 4573.5 | 0.3673 | $^{125}$Xe | 1408.0 | 2301.5 | 893.50 | 0.2578 |
| $^{132}$Xe | 4746.6 | 8935.2 | 4188.6 | 0.3602 | $^{130}$Xe | 1059.7 | 3688.1 | 2628.4 | 0.2549 |
| $^{132}$Xe | 6346.5 | 8935.2 | 2588.7 | 0.3597 | $^{130}$Xe | 5362.5 | 9255.8 | 3893.4 | 0.2488 |
| $^{125}$Xe | 938.57 | 3210.8 | 2272.2 | 0.3480 | $^{125}$Xe | 651.05 | 1387.9 | 736.85 | 0.2444 |
| $^{125}$Xe | 660.05 | 3210.8 | 2550.8 | 0.3480 | $^{125}$Xe | 688.32 | 1718.6 | 1030.3 | 0.2424 |
| $^{130}$Xe | 2762.9 | 3299.0 | 536.09 | 0.3426 | $^{125}$Xe | 546.55 | 1030.3 | 483.70 | 0.2410 |
| $^{132}$Xe | 2575.7 | 3243.4 | 667.72 | 0.3414 | $^{130}$Xe | 1706.9 | 2243.0 | 536.09 | 0.2379 |
| $^{131}$Xe | 163.93 | 163.93 | 0.0 | 0.3390 | $^{125}$Xe | 519.10 | 3619.0 | 3099.9 | 0.2376 |
| $^{131}$Xe | 642.00 | 805.93 | 163.93 | 0.3390 | $^{125}$Xe | 5218.6 | 7603.3 | 2384.7 | 0.2373 |
| $^{130}$Xe | 2886.0 | 2886.0 | 0.0 | 0.3269 | $^{132}$Xe | 1456.5 | 2754.4 | 1297.9 | 0.2371 |
| $^{130}$Xe | 1257.5 | 1793.5 | 536.09 | 0.3209 | $^{130}$Xe | 209.00 | 3535.2 | 3326.2 | 0.2344 |
| $^{132}$Xe | 1669.7 | 4094.5 | 2424.8 | 0.3199 | $^{125}$Xe | 686.37 | 1579.9 | 893.50 | 0.2344 |
| $^{132}$Xe | 506.11 | 2469.1 | 1963.0 | 0.3145 | $^{132}$Xe | 1295.3 | 1963.0 | 667.72 | 0.2326 |

continues on next page

Table B.4: Number of gammas per 100 thermal neutron captures in $^{nat}$Xe

continued from previous page

| Xenon isotope | Gamma energy (keV) | From level (keV) | To level (keV) | $I_\gamma$ per 100 captures | Xenon isotope | Gamma energy (keV) | From level (keV) | To level (keV) | $I_\gamma$ per 100 captures |
|---|---|---|---|---|---|---|---|---|---|
| $^{131}$Xe | 810.37 | 1616.3 | 805.93 | 0.3102 | $^{133}$Xe | 856.28 | 1386.2 | 529.87 | 0.2309 |
| $^{125}$Xe | 5348.4 | 7603.3 | 2255.0 | 0.2974 | $^{133}$Xe | 4696.3 | 6440.1 | 1743.8 | 0.2309 |
| $^{132}$Xe | 1297.9 | 1297.9 | 0.0 | 0.2937 | $^{133}$Xe | 357.60 | 1743.8 | 1386.2 | 0.2309 |
| $^{130}$Xe | 5567.7 | 9255.8 | 3688.1 | 0.2893 | $^{130}$Xe | 399.56 | 2841.6 | 2442.0 | 0.2269 |
| $^{131}$Xe | 189.00 | 1805.3 | 1616.3 | 0.2881 | $^{125}$Xe | 591.28 | 1387.9 | 796.62 | 0.2249 |
| $^{132}$Xe | 1314.1 | 2754.4 | 1440.3 | 0.2871 | $^{130}$Xe | 677.53 | 4370.7 | 3693.2 | 0.2244 |
| $^{125}$Xe | 640.90 | 893.50 | 252.60 | 0.2840 | $^{130}$Xe | 4908.7 | 9255.8 | 4347.1 | 0.2244 |
| $^{132}$Xe | 1719.5 | 4188.6 | 2469.1 | 0.2781 | $^{130}$Xe | 4885.1 | 9255.8 | 4370.7 | 0.2244 |
| $^{130}$Xe | 2092.3 | 2628.4 | 536.09 | 0.2775 | $^{125}$Xe | 371.92 | 483.70 | 111.78 | 0.2216 |
| $^{131}$Xe | 670.20 | 1641.4 | 971.22 | 0.2726 | $^{125}$Xe | 832.18 | 2550.8 | 1718.6 | 0.2207 |
| $^{132}$Xe | 1372.1 | 2670.0 | 1297.9 | 0.2718 | $^{130}$Xe | 6493.2 | 9255.8 | 2762.6 | 0.2171 |
| $^{125}$Xe | 996.60 | 5067.5 | 4070.9 | 0.2690 | $^{132}$Xe | 910.68 | 2714.4 | 1803.7 | 0.2167 |
| $^{125}$Xe | 2535.8 | 7603.3 | 5067.5 | 0.2690 | $^{129}$Xe | 196.56 | 236.14 | 39.578 | 0.2135 |
| $^{125}$Xe | 582.96 | 893.50 | 310.54 | 0.2670 | $^{125}$Xe | 5031.2 | 7603.3 | 2572.1 | 0.2054 |
| $^{133}$Xe | 529.87 | 529.87 | 0.0 | 0.2665 | $^{125}$Xe | 1130.9 | 2572.1 | 1441.2 | 0.2054 |
| $^{125}$Xe | 804.87 | 2384.7 | 1579.9 | 0.2047 | $^{132}$Xe | 363.39 | 1803.7 | 1440.3 | 0.1369 |
| $^{132}$Xe | 621.06 | 2424.8 | 1803.7 | 0.2021 | $^{125}$Xe | 1378.1 | 2819.3 | 1441.2 | 0.1369 |
| $^{130}$Xe | 6550.9 | 9255.8 | 2704.9 | 0.2005 | $^{133}$Xe | 1052.3 | 1052.3 | 0.0 | 0.1360 |
| $^{130}$Xe | 6869.6 | 9255.8 | 2386.2 | 0.1955 | $^{129}$Xe | 534.97 | 771.11 | 236.14 | 0.1343 |
| $^{130}$Xe | 539.11 | 2171.6 | 1632.5 | 0.1896 | $^{130}$Xe | 252.80 | 2886.0 | 2633.2 | 0.1340 |
| $^{130}$Xe | 5361.5 | 9255.8 | 3894.3 | 0.1882 | $^{125}$Xe | 807.54 | 3619.0 | 2811.5 | 0.1331 |
| $^{130}$Xe | 6012.9 | 9255.8 | 3242.9 | 0.1880 | $^{125}$Xe | 312.40 | 4383.3 | 4070.9 | 0.1328 |
| $^{130}$Xe | 1019.9 | 3406.1 | 2386.2 | 0.1824 | $^{125}$Xe | 4223.8 | 7603.3 | 3379.5 | 0.1311 |
| $^{125}$Xe | 43.260 | 295.86 | 252.60 | 0.1814 | $^{130}$Xe | 351.14 | 3893.4 | 3542.2 | 0.1298 |
| $^{130}$Xe | 6104.5 | 9255.8 | 3151.3 | 0.1810 | $^{130}$Xe | 2870.0 | 3406.1 | 536.09 | 0.1295 |
| $^{130}$Xe | 2100.8 | 3894.3 | 1793.5 | 0.1759 | $^{132}$Xe | 1290.8 | 2588.7 | 1297.9 | 0.1269 |
| $^{130}$Xe | 961.41 | 2978.5 | 2017.1 | 0.1754 | $^{132}$Xe | 947.86 | 3058.1 | 2110.3 | 0.1258 |
| $^{130}$Xe | 1096.4 | 1632.5 | 536.09 | 0.1720 | $^{129}$Xe | 624.42 | 1395.5 | 771.11 | 0.1251 |
| $^{125}$Xe | 304.40 | 3379.5 | 3075.1 | 0.1710 | $^{129}$Xe | 576.67 | 1972.2 | 1395.5 | 0.1251 |
| $^{130}$Xe | 6596.4 | 9255.8 | 2659.4 | 0.1686 | $^{129}$Xe | 4935.6 | 6907.8 | 1972.2 | 0.1251 |

continues on next page

Table B.4: Number of gammas per 100 thermal neutron captures in $^{nat}$Xe

continued from previous page

| Xenon isotope | Gamma energy (keV) | From level (keV) | To level (keV) | $I_\gamma$ per 100 captures | Xenon isotope | Gamma energy (keV) | From level (keV) | To level (keV) | $I_\gamma$ per 100 captures |
|---|---|---|---|---|---|---|---|---|---|
| $^{132}$Xe | 1760.2 | 3058.1 | 1297.9 | 0.1677 | $^{132}$Xe | 2002.3 | 2670.0 | 667.72 | 0.1250 |
| $^{132}$Xe | 1254.4 | 3058.1 | 1803.7 | 0.1677 | $^{125}$Xe | 748.80 | 4268.2 | 3519.4 | 0.1238 |
| $^{130}$Xe | 162.70 | 2386.2 | 2223.5 | 0.1646 | $^{125}$Xe | 3335.1 | 7603.3 | 4268.2 | 0.1238 |
| $^{131}$Xe | 4963.7 | 6605.1 | 1641.4 | 0.1628 | $^{125}$Xe | 4784.1 | 7603.3 | 2819.3 | 0.1228 |
| $^{130}$Xe | 137.10 | 3326.2 | 3189.1 | 0.1615 | $^{130}$Xe | 6711.4 | 9255.8 | 2544.5 | 0.1200 |
| $^{133}$Xe | 5387.8 | 6440.1 | 1052.3 | 0.1608 | $^{130}$Xe | 967.03 | 2171.6 | 1204.6 | 0.1195 |
| $^{131}$Xe | 444.00 | 2249.3 | 1805.3 | 0.1599 | $^{130}$Xe | 764.28 | 3461.2 | 2696.9 | 0.1191 |
| $^{131}$Xe | 4355.8 | 6605.1 | 2249.3 | 0.1599 | $^{130}$Xe | 1127.4 | 3299.0 | 2171.6 | 0.1188 |
| $^{130}$Xe | 1610.4 | 3242.9 | 1632.5 | 0.1580 | $^{130}$Xe | 2008.4 | 2544.5 | 536.09 | 0.1181 |
| $^{131}$Xe | 991.60 | 3185.9 | 2194.3 | 0.1570 | $^{130}$Xe | 1727.0 | 3535.2 | 1808.2 | 0.1172 |
| $^{131}$Xe | 389.00 | 2194.3 | 1805.3 | 0.1570 | $^{125}$Xe | 484.25 | 736.85 | 252.60 | 0.1146 |
| $^{131}$Xe | 3419.2 | 6605.1 | 3185.9 | 0.1570 | $^{132}$Xe | 812.36 | 2110.3 | 1297.9 | 0.1128 |
| $^{130}$Xe | 382.43 | 2442.0 | 2059.6 | 0.1543 | $^{130}$Xe | 599.76 | 2659.4 | 2059.6 | 0.1124 |
| $^{125}$Xe | 1162.9 | 2550.8 | 1387.9 | 0.1500 | $^{125}$Xe | 628.89 | 3519.4 | 2890.5 | 0.1115 |
| $^{130}$Xe | 7462.3 | 9255.8 | 1793.5 | 0.1449 | $^{131}$Xe | 655.68 | 2297.1 | 1641.4 | 0.1097 |
| $^{130}$Xe | 686.03 | 1808.2 | 1122.1 | 0.1400 | $^{131}$Xe | 4308.0 | 6605.1 | 2297.1 | 0.1097 |
| $^{125}$Xe | 3220.0 | 7603.3 | 4383.3 | 0.1394 | $^{130}$Xe | 2067.0 | 3189.1 | 1122.1 | 0.1097 |
| $^{132}$Xe | 1921.0 | 2588.7 | 667.72 | 0.1394 | $^{125}$Xe | 5094.6 | 7603.3 | 2508.7 | 0.1086 |
| $^{125}$Xe | 5428.5 | 7603.3 | 2174.8 | 0.1384 | $^{125}$Xe | 1120.8 | 2508.7 | 1387.9 | 0.1086 |
| $^{125}$Xe | 1438.0 | 2174.8 | 736.85 | 0.1384 | $^{130}$Xe | 7012.8 | 9255.8 | 2243.0 | 0.1085 |
| $^{130}$Xe | 7032.3 | 9255.8 | 2223.5 | 0.1084 | $^{130}$Xe | 7238.7 | 9255.8 | 2017.1 | 0.07243 |
| $^{130}$Xe | 1154.6 | 3326.2 | 2171.6 | 0.1077 | $^{125}$Xe | 3310.7 | 7603.3 | 4292.6 | 0.07235 |
| $^{125}$Xe | 5188.5 | 7603.3 | 2414.8 | 0.1076 | $^{125}$Xe | 696.31 | 2006.4 | 1310.1 | 0.07166 |
| $^{130}$Xe | 402.50 | 4942.6 | 4540.1 | 0.1073 | $^{130}$Xe | 470.85 | 2103.4 | 1632.5 | 0.06893 |
| $^{129}$Xe | 732.99 | 1755.3 | 1022.3 | 0.1056 | $^{125}$Xe | 208.41 | 3486.3 | 3277.9 | 0.06826 |
| $^{129}$Xe | 580.11 | 1022.3 | 442.20 | 0.1056 | $^{130}$Xe | 2284.0 | 3406.1 | 1122.1 | 0.06749 |
| $^{129}$Xe | 5152.5 | 6907.8 | 1755.3 | 0.1056 | $^{129}$Xe | 712.08 | 2048.2 | 1336.1 | 0.06718 |
| $^{129}$Xe | 402.62 | 442.20 | 39.578 | 0.1056 | $^{129}$Xe | 4859.6 | 6907.8 | 2048.2 | 0.06718 |
| $^{125}$Xe | 4452.2 | 7603.3 | 3151.1 | 0.1032 | $^{130}$Xe | 937.21 | 2954.3 | 2017.1 | 0.06658 |
| $^{130}$Xe | 1500.3 | 2704.9 | 1204.6 | 0.1023 | $^{135}$Xe | 4231.0 | 6382.5 | 2151.5 | 0.06603 |

continues on next page

Table B.4: Number of gammas per 100 thermal neutron captures in $^{nat}$Xe

continued from previous page

| Xenon isotope | Gamma energy (keV) | From level (keV) | To level (keV) | $I_\gamma$ per 100 captures | Xenon isotope | Gamma energy (keV) | From level (keV) | To level (keV) | $I_\gamma$ per 100 captures |
|---|---|---|---|---|---|---|---|---|---|
| $^{130}$Xe | 5475.3 | 9255.8 | 3780.5 | 0.1013 | $^{135}$Xe | 2151.5 | 2151.5 | 0.0 | 0.06603 |
| $^{125}$Xe | 675.09 | 2255.0 | 1579.9 | 0.09913 | $^{130}$Xe | 499.78 | 2886.0 | 2386.2 | 0.06537 |
| $^{125}$Xe | 867.06 | 2255.0 | 1387.9 | 0.09913 | $^{130}$Xe | 5794.6 | 9255.8 | 3461.2 | 0.06440 |
| $^{125}$Xe | 669.46 | 2255.0 | 1585.5 | 0.09913 | $^{125}$Xe | 778.80 | 2166.7 | 1387.9 | 0.06224 |
| $^{130}$Xe | 1272.1 | 1808.2 | 536.09 | 0.09797 | $^{125}$Xe | 3550.5 | 7603.3 | 4052.8 | 0.06163 |
| $^{132}$Xe | 669.95 | 2110.3 | 1440.3 | 0.09479 | $^{125}$Xe | 4325.4 | 7603.3 | 3277.9 | 0.06112 |
| $^{130}$Xe | 756.04 | 4217.2 | 3461.2 | 0.09403 | $^{125}$Xe | 783.25 | 1579.9 | 796.62 | 0.06093 |
| $^{130}$Xe | 5929.6 | 9255.8 | 3326.2 | 0.09403 | $^{133}$Xe | 5089.7 | 6440.1 | 1350.4 | 0.05936 |
| $^{130}$Xe | 5267.4 | 9255.8 | 3988.4 | 0.09403 | $^{132}$Xe | 431.91 | 2394.9 | 1963.0 | 0.05877 |
| $^{130}$Xe | 5038.6 | 9255.8 | 4217.2 | 0.09403 | $^{132}$Xe | 687.73 | 1985.7 | 1297.9 | 0.05875 |
| $^{125}$Xe | 805.02 | 2811.5 | 2006.4 | 0.09400 | $^{130}$Xe | 338.65 | 2442.0 | 2103.4 | 0.05865 |
| $^{125}$Xe | 519.20 | 3898.7 | 3379.5 | 0.09296 | $^{130}$Xe | 981.10 | 3959.6 | 2978.5 | 0.05791 |
| $^{125}$Xe | 3704.6 | 7603.3 | 3898.7 | 0.09296 | $^{130}$Xe | 9255.8 | 9255.8 | 0.0 | 0.05791 |
| $^{132}$Xe | 889.30 | 2187.2 | 1297.9 | 0.08787 | $^{130}$Xe | 5296.2 | 9255.8 | 3959.6 | 0.05791 |
| $^{130}$Xe | 806.86 | 2978.5 | 2171.6 | 0.08772 | $^{130}$Xe | 5278.5 | 9255.8 | 3977.3 | 0.05791 |
| $^{132}$Xe | 284.63 | 2394.9 | 2110.3 | 0.08707 | $^{125}$Xe | 344.16 | 596.76 | 252.60 | 0.05754 |
| $^{125}$Xe | 573.28 | 1310.1 | 736.85 | 0.08668 | $^{125}$Xe | 878.89 | 3151.1 | 2272.2 | 0.05687 |
| $^{130}$Xe | 825.02 | 2633.2 | 1808.2 | 0.08546 | $^{125}$Xe | 618.28 | 2890.5 | 2272.2 | 0.05651 |
| $^{130}$Xe | 603.57 | 1808.2 | 1204.6 | 0.08118 | $^{130}$Xe | 313.40 | 2659.4 | 2346.0 | 0.05619 |
| $^{132}$Xe | 8935.2 | 8935.2 | 0.0 | 0.08032 | $^{130}$Xe | 286.36 | 2346.0 | 2059.6 | 0.05619 |
| $^{130}$Xe | 2029.2 | 3151.3 | 1122.1 | 0.07959 | $^{125}$Xe | 339.31 | 1209.9 | 870.60 | 0.05596 |
| $^{129}$Xe | 752.69 | 1576.0 | 823.31 | 0.07919 | $^{125}$Xe | 858.97 | 3131.2 | 2272.2 | 0.05556 |
| $^{129}$Xe | 587.17 | 823.31 | 236.14 | 0.07919 | $^{130}$Xe | 894.50 | 3780.5 | 2886.0 | 0.05519 |
| $^{132}$Xe | 984.45 | 2424.8 | 1440.3 | 0.07679 | $^{130}$Xe | 735.52 | 2978.5 | 2243.0 | 0.05482 |
| $^{130}$Xe | 1389.0 | 3406.1 | 2017.1 | 0.07661 | $^{125}$Xe | 806.30 | 4292.6 | 3486.3 | 0.05481 |
| $^{130}$Xe | 896.74 | 2704.9 | 1808.2 | 0.05421 | $^{125}$Xe | 524.35 | 3075.1 | 2550.8 | 0.03528 |
| $^{125}$Xe | 555.73 | 2414.8 | 1859.1 | 0.05379 | $^{131}$Xe | 636.99 | 636.99 | 0.0 | 0.03525 |
| $^{125}$Xe | 1618.2 | 2414.8 | 796.62 | 0.05379 | $^{130}$Xe | 1181.6 | 2386.2 | 1204.6 | 0.03480 |
| $^{125}$Xe | 248.30 | 3379.5 | 3131.2 | 0.05303 | $^{132}$Xe | 2148.2 | 4188.6 | 2040.4 | 0.03477 |
| $^{125}$Xe | 331.87 | 3151.1 | 2819.3 | 0.05175 | $^{130}$Xe | 1054.9 | 3688.1 | 2633.2 | 0.03441 |

continues on next page

Table B.4: Number of gammas per 100 thermal neutron captures in $^{nat}$Xe

continued from previous page

| Xenon isotope | Gamma energy (keV) | From level (keV) | To level (keV) | $I_\gamma$ per 100 captures | Xenon isotope | Gamma energy (keV) | From level (keV) | To level (keV) | $I_\gamma$ per 100 captures |
|---|---|---|---|---|---|---|---|---|---|
| $^{130}$Xe | 671.39 | 1793.5 | 1122.1 | 0.05134 | $^{130}$Xe | 855.20 | 3151.3 | 2296.1 | 0.03382 |
| $^{127}$Xe | 124.75 | 124.75 | 0.0 | 0.05126 | $^{129}$Xe | 817.42 | 1336.1 | 518.70 | 0.03359 |
| $^{125}$Xe | 595.74 | 2811.5 | 2215.7 | 0.04982 | $^{129}$Xe | 670.70 | 1336.1 | 665.42 | 0.03359 |
| $^{132}$Xe | 2384.9 | 4188.6 | 1803.7 | 0.04728 | $^{125}$Xe | 625.44 | 2550.8 | 1925.3 | 0.03310 |
| $^{130}$Xe | 2344.8 | 3977.3 | 1632.5 | 0.04596 | $^{133}$Xe | 733.97 | 1609.3 | 875.33 | 0.03263 |
| $^{125}$Xe | 548.94 | 1859.1 | 1310.1 | 0.04539 | $^{133}$Xe | 452.70 | 2062.0 | 1609.3 | 0.03263 |
| $^{131}$Xe | 80.185 | 80.185 | 0.0 | 0.04438 | $^{133}$Xe | 4378.1 | 6440.1 | 2062.0 | 0.03263 |
| $^{131}$Xe | 284.30 | 364.49 | 80.185 | 0.04438 | $^{130}$Xe | 1987.0 | 3780.5 | 1793.5 | 0.03246 |
| $^{130}$Xe | 622.96 | 2704.9 | 2082.0 | 0.04398 | $^{125}$Xe | 273.84 | 870.60 | 596.76 | 0.03243 |
| $^{132}$Xe | 784.98 | 2588.7 | 1803.7 | 0.04321 | $^{130}$Xe | 1614.1 | 2150.2 | 536.09 | 0.03223 |
| $^{130}$Xe | 2615.2 | 3151.3 | 536.09 | 0.04298 | $^{133}$Xe | 875.33 | 875.33 | 0.0 | 0.03190 |
| $^{125}$Xe | 618.54 | 2006.4 | 1387.9 | 0.04228 | $^{125}$Xe | 202.79 | 3277.9 | 3075.1 | 0.03168 |
| $^{125}$Xe | 908.40 | 3075.1 | 2166.7 | 0.04150 | $^{129}$Xe | 604.00 | 2180.0 | 1576.0 | 0.03160 |
| $^{125}$Xe | 848.65 | 1585.5 | 736.85 | 0.04046 | $^{129}$Xe | 4727.8 | 6907.8 | 2180.0 | 0.03160 |
| $^{125}$Xe | 725.52 | 2166.7 | 1441.2 | 0.03983 | $^{125}$Xe | 370.96 | 3075.1 | 2704.1 | 0.03154 |
| $^{130}$Xe | 7447.6 | 9255.8 | 1808.2 | 0.03975 | $^{125}$Xe | 997.60 | 4052.8 | 3055.2 | 0.03097 |
| $^{130}$Xe | 488.83 | 3461.2 | 2972.3 | 0.03931 | $^{125}$Xe | 943.56 | 2384.7 | 1441.2 | 0.03070 |
| $^{130}$Xe | 877.35 | 2082.0 | 1204.6 | 0.03927 | $^{132}$Xe | 1148.4 | 2588.7 | 1440.3 | 0.03067 |
| $^{132}$Xe | 1757.1 | 2424.8 | 667.72 | 0.03799 | $^{125}$Xe | 952.90 | 4052.8 | 3099.9 | 0.03066 |
| $^{130}$Xe | 1745.4 | 3988.4 | 2243.0 | 0.03791 | $^{130}$Xe | 5632.9 | 9255.8 | 3622.9 | 0.02905 |
| $^{129}$Xe | 479.12 | 518.70 | 39.578 | 0.03762 | $^{130}$Xe | 1760.0 | 2296.1 | 536.09 | 0.02889 |
| $^{130}$Xe | 908.32 | 3151.3 | 2243.0 | 0.03661 | $^{131}$Xe | 794.67 | 1600.6 | 805.93 | 0.02881 |
| $^{130}$Xe | 1176.0 | 3326.2 | 2150.2 | 0.03661 | $^{131}$Xe | 204.70 | 1805.3 | 1600.6 | 0.02881 |
| $^{125}$Xe | 335.35 | 335.35 | 0.0 | 0.03650 | $^{125}$Xe | 148.35 | 483.70 | 335.35 | 0.02881 |
| $^{130}$Xe | 8719.7 | 9255.8 | 536.09 | 0.03612 | $^{132}$Xe | 1442.6 | 2110.3 | 667.72 | 0.02866 |
| $^{130}$Xe | 642.49 | 4184.7 | 3542.2 | 0.03612 | $^{125}$Xe | 802.87 | 3075.1 | 2272.2 | 0.02822 |
| $^{130}$Xe | 5071.1 | 9255.8 | 4184.7 | 0.03612 | $^{132}$Xe | 1617.8 | 3058.1 | 1440.3 | 0.02727 |
| $^{132}$Xe | 2187.2 | 2187.2 | 0.0 | 0.03594 | $^{129}$Xe | 870.30 | 2446.3 | 1576.0 | 0.02724 |
| $^{125}$Xe | 723.81 | 2890.5 | 2166.7 | 0.03560 | $^{129}$Xe | 4461.5 | 6907.8 | 2446.3 | 0.02724 |
| $^{131}$Xe | 334.23 | 971.22 | 636.99 | 0.03556 | $^{125}$Xe | 458.64 | 3277.9 | 2819.3 | 0.02661 |

continues on next page

Table B.4: Number of gammas per 100 thermal neutron captures in $^{nat}$Xe

continued from previous page

| Xenon isotope | Gamma energy (keV) | From level (keV) | To level (keV) | $I_\gamma$ per 100 captures | Xenon isotope | Gamma energy (keV) | From level (keV) | To level (keV) | $I_\gamma$ per 100 captures |
|---|---|---|---|---|---|---|---|---|---|
| $^{125}$Xe | 573.75 | 3277.9 | 2704.1 | 0.02598 | $^{125}$Xe | 1062.2 | 3277.9 | 2215.7 | 0.01774 |
| $^{130}$Xe | 427.92 | 1632.5 | 1204.6 | 0.02593 | $^{137}$Xe | 1218.0 | 1218.0 | 0.0 | 0.01731 |
| $^{125}$Xe | 188.83 | 796.62 | 607.79 | 0.02581 | $^{125}$Xe | 898.13 | 2616.7 | 1718.6 | 0.01642 |
| $^{135}$Xe | 3904.6 | 6382.5 | 2477.9 | 0.02563 | $^{125}$Xe | 504.04 | 2819.3 | 2315.2 | 0.01642 |
| $^{125}$Xe | 416.63 | 1310.1 | 893.50 | 0.02514 | $^{125}$Xe | 202.55 | 2819.3 | 2616.7 | 0.01642 |
| $^{125}$Xe | 692.00 | 1585.5 | 893.50 | 0.02509 | $^{125}$Xe | 654.25 | 919.84 | 265.59 | 0.01606 |
| $^{125}$Xe | 888.50 | 3055.2 | 2166.7 | 0.02376 | $^{127}$Xe | 670.77 | 1751.6 | 1080.8 | 0.01590 |
| $^{135}$Xe | 288.46 | 288.46 | 0.0 | 0.02316 | $^{127}$Xe | 684.83 | 2307.1 | 1622.3 | 0.01546 |
| $^{135}$Xe | 2189.4 | 2477.9 | 288.46 | 0.02307 | $^{127}$Xe | 471.80 | 2778.9 | 2307.1 | 0.01546 |
| $^{125}$Xe | 286.22 | 596.76 | 310.54 | 0.02302 | $^{130}$Xe | 837.10 | 3988.4 | 3151.3 | 0.01517 |
| $^{133}$Xe | 820.51 | 1350.4 | 529.87 | 0.02293 | $^{129}$Xe | 318.18 | 318.18 | 0.0 | 0.01506 |
| $^{130}$Xe | 697.82 | 3326.2 | 2628.4 | 0.02261 | $^{127}$Xe | 5189.8 | 7223.0 | 2033.2 | 0.01451 |
| $^{127}$Xe | 217.48 | 342.23 | 124.75 | 0.02260 | $^{129}$Xe | 343.71 | 665.42 | 321.71 | 0.01434 |
| $^{130}$Xe | 1481.0 | 2017.1 | 536.09 | 0.02248 | $^{125}$Xe | 378.30 | 2384.7 | 2006.4 | 0.01433 |
| $^{133}$Xe | 1350.4 | 1350.4 | 0.0 | 0.02223 | $^{125}$Xe | 1518.6 | 2315.2 | 796.62 | 0.01428 |
| $^{131}$Xe | 4988.8 | 6605.1 | 1616.3 | 0.02211 | $^{137}$Xe | 1937.5 | 4025.5 | 2088.0 | 0.01416 |
| $^{127}$Xe | 595.94 | 938.17 | 342.23 | 0.02115 | $^{127}$Xe | 550.48 | 1080.8 | 530.31 | 0.01407 |
| $^{125}$Xe | 665.66 | 1585.5 | 919.84 | 0.02104 | $^{130}$Xe | 132.03 | 2442.0 | 2310.0 | 0.01389 |
| $^{130}$Xe | 1355.2 | 3988.4 | 2633.2 | 0.02085 | $^{129}$Xe | 5493.5 | 6907.8 | 1414.3 | 0.01377 |
| $^{127}$Xe | 684.10 | 1622.3 | 938.17 | 0.02081 | $^{127}$Xe | 308.98 | 308.98 | 0.0 | 0.01371 |
| $^{125}$Xe | 355.19 | 607.79 | 252.60 | 0.02069 | $^{130}$Xe | 826.20 | 3780.5 | 2954.3 | 0.01364 |
| $^{125}$Xe | 268.50 | 2819.3 | 2550.8 | 0.02053 | $^{125}$Xe | 674.79 | 2890.5 | 2215.7 | 0.01356 |
| $^{129}$Xe | 5331.8 | 6907.8 | 1576.0 | 0.02036 | $^{127}$Xe | 405.56 | 530.31 | 124.75 | 0.01301 |
| $^{132}$Xe | 478.42 | 2588.7 | 2110.3 | 0.01952 | $^{130}$Xe | 2544.5 | 2544.5 | 0.0 | 0.01299 |
| $^{125}$Xe | 839.48 | 3055.2 | 2215.7 | 0.01948 | $^{127}$Xe | 519.11 | 828.09 | 308.98 | 0.01279 |
| $^{129}$Xe | 347.24 | 665.42 | 318.18 | 0.01937 | $^{125}$Xe | 473.40 | 3959.7 | 3486.3 | 0.01261 |
| $^{125}$Xe | 513.51 | 1310.1 | 796.62 | 0.01907 | $^{125}$Xe | 332.90 | 4292.6 | 3959.7 | 0.01261 |
| $^{130}$Xe | 1449.4 | 3242.9 | 1793.5 | 0.01896 | $^{135}$Xe | 4127.0 | 6382.5 | 2255.5 | 0.01257 |
| $^{129}$Xe | 282.13 | 321.71 | 39.578 | 0.01872 | $^{125}$Xe | 561.06 | 1585.5 | 1024.4 | 0.01254 |
| $^{133}$Xe | 262.70 | 262.70 | 0.0 | 0.01843 | $^{125}$Xe | 690.36 | 3075.1 | 2384.7 | 0.01245 |

continues on next page

Table B.4: Number of gammas per 100 thermal neutron captures in $^{nat}$Xe

continued from previous page

| Xenon isotope | Gamma energy (keV) | From level (keV) | To level (keV) | $I_\gamma$ per 100 captures | Xenon isotope | Gamma energy (keV) | From level (keV) | To level (keV) | $I_\gamma$ per 100 captures |
|---|---|---|---|---|---|---|---|---|---|
| $^{129}$Xe | 4871.6 | 6907.8 | 2036.2 | 0.01842 | $^{133}$Xe | 789.60 | 1052.3 | 262.70 | 0.01237 |
| $^{125}$Xe | 12.990 | 265.59 | 252.60 | 0.01813 | $^{130}$Xe | 915.80 | 3894.3 | 2978.5 | 0.01232 |
| $^{125}$Xe | 255.85 | 3075.1 | 2819.3 | 0.01785 | $^{125}$Xe | 464.20 | 3519.4 | 3055.2 | 0.01227 |
| $^{125}$Xe | 859.38 | 3075.1 | 2215.7 | 0.01784 | $^{125}$Xe | 565.26 | 2006.4 | 1441.2 | 0.01218 |
| $^{125}$Xe | 812.81 | 2819.3 | 2006.4 | 0.01779 | $^{130}$Xe | 363.46 | 2171.6 | 1808.2 | 0.01214 |
| $^{125}$Xe | 466.65 | 2890.5 | 2423.9 | 0.01187 | $^{137}$Xe | 870.00 | 2088.0 | 1218.0 | 0.00762 |
| $^{125}$Xe | 269.74 | 1579.9 | 1310.1 | 0.01172 | $^{125}$Xe | 192.92 | 1030.3 | 837.33 | 0.00723 |
| $^{130}$Xe | 698.45 | 3242.9 | 2544.5 | 0.01106 | $^{129}$Xe | 592.11 | 1414.3 | 822.16 | 0.00688 |
| $^{125}$Xe | 893.94 | 2819.3 | 1925.3 | 0.01095 | $^{129}$Xe | 324.79 | 1414.3 | 1089.5 | 0.00688 |
| $^{127}$Xe | 4444.1 | 7223.0 | 2778.9 | 0.01091 | $^{127}$Xe | 218.00 | 3620.8 | 3402.8 | 0.00684 |
| $^{125}$Xe | 386.90 | 870.60 | 483.70 | 0.01081 | $^{133}$Xe | 680.26 | 680.26 | 0.0 | 0.00680 |
| $^{125}$Xe | 466.43 | 3277.9 | 2811.5 | 0.01077 | $^{125}$Xe | 105.10 | 3075.1 | 2970.0 | 0.00664 |
| $^{130}$Xe | 916.92 | 3988.4 | 3071.5 | 0.01062 | $^{127}$Xe | 172.35 | 297.10 | 124.75 | 0.00660 |
| $^{127}$Xe | 3820.2 | 7223.0 | 3402.8 | 0.01057 | $^{127}$Xe | 5249.4 | 7223.0 | 1973.6 | 0.00657 |
| $^{125}$Xe | 505.95 | 1536.2 | 1030.3 | 0.01056 | $^{127}$Xe | 1561.6 | 1973.6 | 411.97 | 0.00657 |
| $^{125}$Xe | 326.29 | 1536.2 | 1209.9 | 0.01056 | $^{137}$Xe | 867.93 | 2088.0 | 1220.1 | 0.00655 |
| $^{130}$Xe | 1814.7 | 3622.9 | 1808.2 | 0.01037 | $^{129}$Xe | 570.78 | 1089.5 | 518.70 | 0.00652 |
| $^{130}$Xe | 206.62 | 2310.0 | 2103.4 | 0.01029 | $^{133}$Xe | 670.12 | 1350.4 | 680.26 | 0.00642 |
| $^{133}$Xe | 522.43 | 1052.3 | 529.87 | 0.01020 | $^{127}$Xe | 637.21 | 1283.1 | 645.90 | 0.00639 |
| $^{137}$Xe | 1220.1 | 1220.1 | 0.0 | 0.01010 | $^{130}$Xe | 765.08 | 3151.3 | 2386.2 | 0.00637 |
| $^{127}$Xe | 680.60 | 1508.7 | 828.09 | 0.00990 | $^{127}$Xe | 734.68 | 2243.4 | 1508.7 | 0.00627 |
| $^{125}$Xe | 771.84 | 1024.4 | 252.60 | 0.00980 | $^{127}$Xe | 411.97 | 411.97 | 0.0 | 0.00624 |
| $^{132}$Xe | 559.73 | 2670.0 | 2110.3 | 0.00978 | $^{125}$Xe | 387.38 | 3277.9 | 2890.5 | 0.00602 |
| $^{135}$Xe | 1131.5 | 1131.5 | 0.0 | 0.00960 | $^{127}$Xe | 746.14 | 2497.7 | 1751.6 | 0.00601 |
| $^{135}$Xe | 1124.0 | 2255.5 | 1131.5 | 0.00958 | $^{133}$Xe | 438.93 | 1350.4 | 911.45 | 0.00596 |
| $^{130}$Xe | 1764.9 | 3988.4 | 2223.5 | 0.00948 | $^{137}$Xe | 1925.5 | 4025.5 | 2100.0 | 0.00589 |
| $^{127}$Xe | 4979.6 | 7223.0 | 2243.4 | 0.00947 | $^{129}$Xe | 500.45 | 822.16 | 321.71 | 0.00584 |
| $^{129}$Xe | 1265.1 | 2036.2 | 771.11 | 0.00921 | $^{137}$Xe | 2034.3 | 4025.5 | 1991.2 | 0.00581 |
| $^{129}$Xe | 1213.2 | 2036.2 | 823.05 | 0.00921 | $^{125}$Xe | 422.41 | 3075.1 | 2652.7 | 0.00581 |
| $^{125}$Xe | 501.98 | 837.33 | 335.35 | 0.00884 | $^{127}$Xe | 1446.1 | 2033.2 | 587.07 | 0.00580 |

continues on next page

Table B.4: Number of gammas per 100 thermal neutron captures in $^{nat}$Xe

continued from previous page

| Xenon isotope | Gamma energy (keV) | From level (keV) | To level (keV) | $I_\gamma$ per 100 captures | Xenon isotope | Gamma energy (keV) | From level (keV) | To level (keV) | $I_\gamma$ per 100 captures |
|---|---|---|---|---|---|---|---|---|---|
| $^{130}$Xe | 1451.3 | 3622.9 | 2171.6 | 0.00882 | $^{127}$Xe | 1321.6 | 2033.2 | 711.61 | 0.00580 |
| $^{130}$Xe | 3977.3 | 3977.3 | 0.0 | 0.00873 | $^{127}$Xe | 127.00 | 3402.8 | 3275.8 | 0.00580 |
| $^{132}$Xe | 684.36 | 2670.0 | 1985.7 | 0.00870 | $^{127}$Xe | 434.10 | 3402.8 | 2968.7 | 0.00580 |
| $^{125}$Xe | 965.57 | 1859.1 | 893.50 | 0.00862 | $^{127}$Xe | 120.00 | 3402.8 | 3282.8 | 0.00580 |
| $^{132}$Xe | 1727.2 | 2394.9 | 667.72 | 0.00826 | $^{125}$Xe | 732.30 | 2970.0 | 2237.7 | 0.00577 |
| $^{129}$Xe | 278.60 | 318.18 | 39.578 | 0.00813 | $^{137}$Xe | 601.05 | 601.05 | 0.0 | 0.00569 |
| $^{127}$Xe | 3940.2 | 7223.0 | 3282.8 | 0.00786 | $^{127}$Xe | 5471.4 | 7223.0 | 1751.6 | 0.00564 |
| $^{127}$Xe | 952.30 | 2968.7 | 2016.4 | 0.00779 | $^{130}$Xe | 985.38 | 3622.9 | 2637.5 | 0.00550 |
| $^{127}$Xe | 733.29 | 2016.4 | 1283.1 | 0.00779 | $^{130}$Xe | 2101.4 | 2637.5 | 536.09 | 0.00550 |
| $^{127}$Xe | 251.90 | 2968.7 | 2716.8 | 0.00779 | $^{132}$Xe | 1097.0 | 2394.9 | 1297.9 | 0.00545 |
| $^{129}$Xe | 321.71 | 321.71 | 0.0 | 0.00543 | $^{125}$Xe | 764.30 | 4383.3 | 3619.0 | 0.00332 |
| $^{125}$Xe | 126.77 | 3277.9 | 3151.1 | 0.00539 | $^{125}$Xe | 1283.4 | 4383.3 | 3099.9 | 0.00332 |
| $^{125}$Xe | 705.29 | 2423.9 | 1718.6 | 0.00526 | $^{127}$Xe | 375.46 | 375.46 | 0.0 | 0.00327 |
| $^{127}$Xe | 303.67 | 645.90 | 342.23 | 0.00503 | $^{127}$Xe | 935.00 | 4136.8 | 3201.8 | 0.00327 |
| $^{125}$Xe | 667.24 | 919.84 | 252.60 | 0.00498 | $^{127}$Xe | 889.70 | 3201.8 | 2312.1 | 0.00327 |
| $^{125}$Xe | 157.90 | 4292.6 | 4134.7 | 0.00493 | $^{127}$Xe | 803.41 | 2312.1 | 1508.7 | 0.00327 |
| $^{132}$Xe | 147.28 | 2110.3 | 1963.0 | 0.00485 | $^{127}$Xe | 3086.2 | 7223.0 | 4136.8 | 0.00327 |
| $^{125}$Xe | 433.49 | 1030.3 | 596.76 | 0.00482 | $^{130}$Xe | 826.00 | 3977.3 | 3151.3 | 0.00322 |
| $^{130}$Xe | 1545.9 | 2082.0 | 536.09 | 0.00471 | $^{127}$Xe | 776.62 | 2243.4 | 1466.8 | 0.00320 |
| $^{137}$Xe | 773.18 | 1991.2 | 1218.0 | 0.00465 | $^{125}$Xe | 279.20 | 1859.1 | 1579.9 | 0.00318 |
| $^{125}$Xe | 1036.0 | 2423.9 | 1387.9 | 0.00458 | $^{127}$Xe | 462.31 | 587.07 | 124.75 | 0.00307 |
| $^{127}$Xe | 503.90 | 3282.8 | 2778.9 | 0.00455 | $^{132}$Xe | 1126.9 | 2424.8 | 1297.9 | 0.00303 |
| $^{127}$Xe | 785.10 | 3282.8 | 2497.7 | 0.00455 | $^{137}$Xe | 1302.7 | 1302.7 | 0.0 | 0.00303 |
| $^{127}$Xe | 314.10 | 3282.8 | 2968.7 | 0.00455 | $^{137}$Xe | 2100.0 | 2100.0 | 0.0 | 0.00302 |
| $^{137}$Xe | 1512.2 | 1512.2 | 0.0 | 0.00450 | $^{125}$Xe | 887.66 | 2423.9 | 1536.2 | 0.00295 |
| $^{130}$Xe | 736.90 | 3622.9 | 2886.0 | 0.00436 | $^{127}$Xe | 390.06 | 711.61 | 321.55 | 0.00293 |
| $^{132}$Xe | 591.19 | 2394.9 | 1803.7 | 0.00435 | $^{127}$Xe | 1908.4 | 2033.2 | 124.75 | 0.00290 |
| $^{137}$Xe | 608.37 | 4025.5 | 3417.1 | 0.00435 | $^{125}$Xe | 297.25 | 607.79 | 310.54 | 0.00290 |
| $^{137}$Xe | 3417.1 | 3417.1 | 0.0 | 0.00435 | $^{125}$Xe | 784.38 | 3000.1 | 2215.7 | 0.00285 |
| $^{127}$Xe | 3602.2 | 7223.0 | 3620.8 | 0.00426 | $^{125}$Xe | 277.79 | 3277.9 | 3000.1 | 0.00285 |

continues on next page

Table B.4: Number of gammas per 100 thermal neutron captures in $^{nat}$Xe

continued from previous page

| Xenon isotope | Gamma energy (keV) | From level (keV) | To level (keV) | $I_\gamma$ per 100 captures | Xenon isotope | Gamma energy (keV) | From level (keV) | To level (keV) | $I_\gamma$ per 100 captures |
|---|---|---|---|---|---|---|---|---|---|
| $^{127}$Xe | 45.130 | 342.23 | 297.10 | 0.00407 | $^{130}$Xe | 1028.1 | 2150.2 | 1122.1 | 0.00280 |
| $^{137}$Xe | 2513.3 | 4025.5 | 1512.2 | 0.00403 | $^{125}$Xe | 856.81 | 4134.7 | 3277.9 | 0.00273 |
| $^{125}$Xe | 757.02 | 2237.7 | 1480.7 | 0.00401 | $^{137}$Xe | 2229.4 | 4025.5 | 1796.1 | 0.00267 |
| $^{127}$Xe | 965.24 | 2716.8 | 1751.6 | 0.00390 | $^{129}$Xe | 548.96 | 588.53 | 39.578 | 0.00259 |
| $^{127}$Xe | 1094.5 | 2716.8 | 1622.3 | 0.00390 | $^{125}$Xe | 643.35 | 1480.7 | 837.33 | 0.00259 |
| $^{127}$Xe | 4254.3 | 7223.0 | 2968.7 | 0.00377 | $^{135}$Xe | 2477.9 | 2477.9 | 0.0 | 0.00256 |
| $^{129}$Xe | 196.99 | 518.70 | 321.71 | 0.00376 | $^{127}$Xe | 587.07 | 587.07 | 0.0 | 0.00254 |
| $^{125}$Xe | 1485.4 | 2926.6 | 1441.2 | 0.00374 | $^{125}$Xe | 325.32 | 3277.9 | 2952.6 | 0.00254 |
| $^{125}$Xe | 148.50 | 3075.1 | 2926.6 | 0.00374 | $^{125}$Xe | 146.69 | 3277.9 | 3131.2 | 0.00253 |
| $^{130}$Xe | 2296.1 | 2296.1 | 0.0 | 0.00370 | $^{125}$Xe | 1264.8 | 2652.7 | 1387.9 | 0.00243 |
| $^{129}$Xe | 411.55 | 823.05 | 411.50 | 0.00362 | $^{127}$Xe | 348.80 | 645.90 | 297.10 | 0.00241 |
| $^{129}$Xe | 504.87 | 823.05 | 318.18 | 0.00362 | $^{127}$Xe | 321.55 | 321.55 | 0.0 | 0.00239 |
| $^{129}$Xe | 234.52 | 823.05 | 588.53 | 0.00362 | $^{127}$Xe | 468.00 | 4088.8 | 3620.8 | 0.00236 |
| $^{130}$Xe | 250.40 | 2310.0 | 2059.6 | 0.00360 | $^{133}$Xe | 372.04 | 1052.3 | 680.26 | 0.00231 |
| $^{125}$Xe | 793.62 | 2652.7 | 1859.1 | 0.00338 | $^{133}$Xe | 648.75 | 911.45 | 262.70 | 0.00228 |
| $^{125}$Xe | 187.84 | 483.70 | 295.86 | 0.00222 | $^{133}$Xe | 417.56 | 680.26 | 262.70 | 0.00161 |
| $^{125}$Xe | 648.40 | 4134.7 | 3486.3 | 0.00221 | $^{129}$Xe | 411.50 | 411.50 | 0.0 | 0.00159 |
| $^{125}$Xe | 223.57 | 335.35 | 111.78 | 0.00219 | $^{130}$Xe | 2150.2 | 2150.2 | 0.0 | 0.00151 |
| $^{129}$Xe | 371.92 | 411.50 | 39.578 | 0.00218 | $^{137}$Xe | 2722.7 | 4025.5 | 1302.7 | 0.00146 |
| $^{132}$Xe | 707.01 | 2670.0 | 1963.0 | 0.00217 | $^{127}$Xe | 880.73 | 3275.8 | 2395.1 | 0.00145 |
| $^{127}$Xe | 638.66 | 1466.8 | 828.09 | 0.00216 | $^{127}$Xe | 778.10 | 3275.8 | 2497.7 | 0.00145 |
| $^{137}$Xe | 3424.4 | 4025.5 | 601.05 | 0.00215 | $^{127}$Xe | 772.80 | 2395.1 | 1622.3 | 0.00145 |
| $^{127}$Xe | 3134.2 | 7223.0 | 4088.8 | 0.00215 | $^{127}$Xe | 611.20 | 3275.8 | 2664.6 | 0.00145 |
| $^{125}$Xe | 1005.1 | 2315.2 | 1310.1 | 0.00214 | $^{127}$Xe | 307.10 | 3275.8 | 2968.7 | 0.00145 |
| $^{137}$Xe | 881.97 | 2100.0 | 1218.0 | 0.00211 | $^{137}$Xe | 576.01 | 1796.1 | 1220.1 | 0.00142 |
| $^{137}$Xe | 2309.9 | 4025.5 | 1715.6 | 0.00208 | $^{127}$Xe | 344.94 | 1283.1 | 938.17 | 0.00140 |
| $^{125}$Xe | 342.20 | 607.79 | 265.59 | 0.00207 | $^{125}$Xe | 163.46 | 3486.3 | 3322.8 | 0.00137 |
| $^{137}$Xe | 385.15 | 986.20 | 601.05 | 0.00193 | $^{137}$Xe | 1534.3 | 1534.3 | 0.0 | 0.00134 |
| $^{137}$Xe | 748.75 | 4025.5 | 3276.7 | 0.00191 | $^{137}$Xe | 1416.7 | 4025.5 | 2608.8 | 0.00134 |
| $^{132}$Xe | 866.29 | 2670.0 | 1803.7 | 0.00190 | $^{127}$Xe | 586.86 | 711.61 | 124.75 | 0.00129 |

continues on next page

Table B.4: Number of gammas per 100 thermal neutron captures in $^{nat}$Xe

continued from previous page

| Xenon isotope | Gamma energy (keV) | From level (keV) | To level (keV) | $I_\gamma$ per 100 captures | Xenon isotope | Gamma energy (keV) | From level (keV) | To level (keV) | $I_\gamma$ per 100 captures |
|---|---|---|---|---|---|---|---|---|---|
| $^{137}$Xe | 1715.6 | 1715.6 | 0.0 | 0.00188 | $^{129}$Xe | 303.46 | 822.16 | 518.70 | 0.00127 |
| $^{125}$Xe | 1633.9 | 3075.1 | 1441.2 | 0.00187 | $^{137}$Xe | 2216.7 | 4025.5 | 1808.8 | 0.00126 |
| $^{133}$Xe | 911.45 | 911.45 | 0.0 | 0.00187 | $^{137}$Xe | 1808.8 | 1808.8 | 0.0 | 0.00126 |
| $^{125}$Xe | 713.90 | 1024.4 | 310.54 | 0.00186 | $^{130}$Xe | 1174.0 | 2296.1 | 1122.1 | 0.00124 |
| $^{127}$Xe | 183.16 | 1080.8 | 897.63 | 0.00183 | $^{125}$Xe | 785.87 | 2952.6 | 2166.7 | 0.00122 |
| $^{133}$Xe | 381.58 | 911.45 | 529.87 | 0.00182 | $^{127}$Xe | 154.85 | 530.31 | 375.46 | 0.00117 |
| $^{133}$Xe | 1087.7 | 1350.4 | 262.70 | 0.00181 | $^{137}$Xe | 1991.2 | 1991.2 | 0.0 | 0.00116 |
| $^{125}$Xe | 1441.1 | 2237.7 | 796.62 | 0.00176 | $^{137}$Xe | 893.25 | 2608.8 | 1715.6 | 0.00112 |
| $^{127}$Xe | 522.17 | 897.63 | 375.46 | 0.00172 | $^{137}$Xe | 578.08 | 1796.1 | 1218.0 | 0.00107 |
| $^{130}$Xe | 227.55 | 2171.6 | 1944.1 | 0.00171 | $^{127}$Xe | 292.27 | 938.17 | 645.90 | 0.00106 |
| $^{129}$Xe | 4735.8 | 6907.8 | 2172.0 | 0.00165 | $^{127}$Xe | 674.38 | 1466.8 | 792.37 | 0.00104 |
| $^{129}$Xe | 1349.0 | 2172.0 | 823.05 | 0.00165 | $^{125}$Xe | 272.44 | 607.79 | 335.35 | 0.00103 |
| $^{137}$Xe | 1573.1 | 4025.5 | 2452.4 | 0.00163 | $^{137}$Xe | 2058.7 | 3276.7 | 1218.0 | 0.00102 |
| $^{137}$Xe | 1466.2 | 2452.4 | 986.20 | 0.00163 | $^{132}$Xe | 306.56 | 2110.3 | 1803.7 | 0.00102 |
| $^{135}$Xe | 2255.5 | 2255.5 | 0.0 | 0.00163 | | | | | |

Table B.4: Number of gammas per 100 thermal neutron captures in $^{nat}$Xe

# Appendix C

# Radiation level in the TPC electronics

ALICE, the dedicated heavy-ion experiment at the CERN LHC [152], will study a variety of colliding systems ranging from pp and pA to light and heavy nuclei.

High beam energy ($Z/A \times 7$ TeV/nucleon) at the LHC combined with high luminosities result in a high primary particle production rate. Many of these particles produce secondaries through hadronic and electromagnetic cascades in the absorbers and structural elements of ALICE. They produce particle fluxes even far away from the interaction point and in shielded regions. Detailed particle transport simulations are needed to calculate the doses and neutron fluences in these regions. These quantities are needed to evaluate the risk of radiation damage and activation of detectors and electronics equipment. Here we will analyze and present the contributions to the radiation background in the region where the ALICE TPC front-end electronics is located concerning the expected particle fluences, fluxes and number of total particles, for a 10 years standard running scenario including Pb–Pb runs.

We also quantify the slow proton background that would originate from a small admixture of $CH_4$ or $N_2$ to the 90% Ne, 10% $CO_2$ TPC gas. All these results were obtained from simulations using the FLUKA transport code.

## C.1 TPC detector and front-end electronics

The Time Projection Chamber (TPC) [154], surrounds the Inner Tracking System (ITS) and is the main tracking detector of the central barrel and together with the ITS, TRD and TOF has to provide charged particle momentum measurement, particle identification and vertex determination with sufficient momentum resolution, two track separation and dE/dx resolution for studies of hadronic and leptonic signals in the region $P_t$<10 GeV/c and pseudorapidities $|\eta|$<0.9. To cover this acceptance the TPC is of cylindrical design with an inner radius of about 80 cm, an outer radius of about 250 cm and an overall length in the beam direction of 500 cm. A gas mixture of 90% Ne, 10% $CO_2$ has been chosen for operating the detector. The front-end electronics have to read out the charge detected by all these pads located on the readout chambers at the TPC end-plates.

The ALICE TPC [155] is a 88 $m^3$ cylinder filled with a gas and divided in two drift regions by the central electrode located at its axial centre. A field cage creates a uniform electric field along each half of the chamber. Charged particles traversing the TPC volume ionise the gas along their path, liberating electrons that drift towards the end plates of the chamber. The necessary signal amplification is provided through avalanche effect in the vicinity of the anode wires. Moving from the anode wire towards the surrounding electrodes, the positive ions created in the avalanche induce a positive current signal on the pad plane. This current signal, which is characterised by a fast rise time (less than 1 ns) and a long tail with a rather complex shape, carries a charge that, for the minimum ionising particle, is of 4.8fC.

The readout of the signal is done by the 570132 pads that form the cathode plane of conventional multi-wire proportional chambers located at the TPC end plates. The signals form the pads are processed by 4356 front-end cards located some 10 cm away form the pad plane via flexible capton cables. In the front-end card a custom made charge sensitive amplifier transforms the charge induced in the pads in a differential semi-gaussian signal that is fed to the input of the ALTRO chip. Each ALTRO contain 16 channels

operating concurrently that digitize and process the input signals. Upon arrival of a first level trigger, the data stream is stored in a memory. The maximum number of samples that can be continuously processed for each trigger (event data stream) is 1000. When the second level trigger (accept or reject) is received, the latest event data stream is either frozen in the data memory, until its complete readout takes place, or discarded. The data memory has the capacity to store up to 8 event data streams. The readout can take place any time, at a speed of 200MByte/sec through a 40-bit wide backplane bus linking the Front End Cards to the Readout Control Unit.

The theoretical predictions for the charged particle multiplicity expected in such collisions range from 2000 up to 8000 charged particles per rapidity unit at mid-rapidity resulting in 80 000 primary charged particles in the central barrel acceptance for the worst case scenario. The expected luminosity of $10^{27}$ cm$^{-2}$s$^{-1}$ will lead to an inelastic event rate of 8 kHz.

The inaccessibility of the ALICE experiment during the entire year of LHC running makes stringent quality tests of the readout electronics mandatory before installation. The radiation load on the TPC is relatively low with a neutron flux received over 10 years of less than $10^{11}$ neutrons/cm$^2$. Thus, standard radiation-soft technologies are suitable for the implementation of this electronics. Nevertheless, some special care should be taken to protect the system against potential damage caused by Single Event Effects (SEEs). Concerning the SEU (Singe Event Upset) in the FPGAs probably only the protons above 10-20 MeV can cause bit-flips. Neutrons can contribue to this effect only if they scatter in the plastic of the chip package or in the PCB with a proton and kick the fast proton into the silicon.

### C.1.1 Detector geometry and scoring

The TPC volume as described in FLUKA is shown in Fig. 9.5 of the Chapter 9. The TPC gas volume is approximated by a cylinder with an inner radius of about 79.25 cm, an outer radius of about 278 cm and an overall length in the beam direction of 550 cm ($-275 < Z < 275cm$). The TPC gas mixture

Table C.1: Dimensions of the scoring layers.

| Layers | Outer radial distance [cm] | Volume [cm$^3$] | Area [cm$^2$] |
|---|---|---|---|
| 1 | 127.20 | 3210.7 | 32107 |
| 2 | 177.20 | 4781.5 | 47815 |
| 3 | 227.20 | 6352.3 | 63523 |
| 4 | 278.17 | 8092.3 | 80923 |

consists of 90% Ne, 10% $CO_2$. There is a correspondence between FLUKA materials and low-energy neutron cross-sections. Since FLUKA low-energy neutron library does not include neon, fluorine has been chosen instead due to its similar properties.

Since the front-end electronics will be placed on the readout chambers at the TPC end-caps, we define 4 concentric cylindrical layers of silicon at radial distances from 77.2 up to 278.17 cm with 1 mm width along the beam direction ($-296.1 < Z < -296cm$ and $284 < Z < 284.1cm$), 10 cm away from the TPC limiting planes. The dimensions of the layers are summarized in Table C.1. We perform two studies for both end-plates (muon-aborber and non-absorber side) considering that are made by aluminium of 1 cm width ($-276 < Z < -275cm$ and $275 < Z < 276cm$). The two scoring regions (muon-aborber and non-absorber side, the right and left group of rings respectively) are shown in Fig. C.1.

Events with average multiplicity of 80 000 primary pions and kaons were transported through the material of the experiment and experimental area which was described with about 3200 volumes.

### C.1.2 Particle fluences based on FLUKA calculations

Firstly we estimate the number of particles in both sides per central event. The results are presented in Tables C.2 and C.3 for the absorber and non-absorber side respectively. In the muon-aborber side there are 45% more neutrons and 40% less charged particles. In both cases most of the neutrons

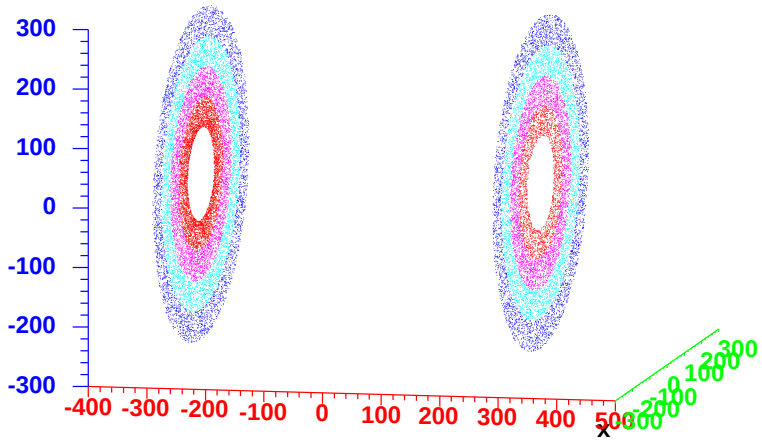


Figure C.1: The two scoring regions (four silicon layers).

come from the muon absorber side as shown in Fig. C.3. The age and energy spectra of the particles that are of main importance for this study can be seen in Figs. C.2 and C.4 respectively.

The way used to calculate particle fluxes in the TPC is via a special tool of FLUKA, the track-length estimator. Defining 4 such estimators, each of them pointing on one silicon layer and taking the average from them during one FLUKA event (one central event), we calculate the total track-length. The track-length is more meaningful than the number of particles, because any signal, or any damage, are proportional to the energy deposited, or to the number of collisions which are all proportional to the track-length. Dividing the total track-length with the volume of the scoring region we obtain the total response or *cumulative fluence* expressed as (particles/cm$^2$/primary).

The results of the FLUKA track-length estimator are always given as differential distributions of fluence in energy (cm$^{-2}$ GeV$^{-1}$ per incident primary unit weight). In figures displaying differential fluence versus energy over a

large range of energy, the abscissa is often the logarithm of energy [144]. In making the coordinate transformation from linear energy and particle-differential fluence distribution $d\Phi/dE$ to logarithmic energy, it is desirable to preserve the fact that relative areas in different energy regions represent relative fluences. This can easily be accomplished by multiplying the conventional particle-differential fluence distribution $d\Phi/dE$ by the energy because $\mathrm{d}\Phi/\mathrm{d}(\log \mathrm{E}) = \mathrm{d}\Phi/(\mathrm{dE/E}) = \mathrm{E}\ \mathrm{d}\Phi/\mathrm{dE}$.

Figures C.5, C.6, C.7, C.8, C.9 and C.10 show the lethargy and kinetic energy spectra of neutrons, all charged particles, protons, pions, kaons and photons respectively. The lethargy spectra are designed to allow visual integration of fluence having the areas under the curves proportional to the fluence. As can be observed, protons, pions and kaons of $E_{\mathrm{kin}} > 10\,\mathrm{MeV}$ can contribute in the fluence. Their respective kinetic energy spectra (same points but both axes are logarithmic) are not very useful but we provide them since is the method of plotting neutron-energy spectra generally chosen.

The particle fluences per central event are shown in Tables C.4 and C.5.

The fluxes (particles/cm$^2$/s) can be obtained from the cumulative fluences by multiplying them with (80000 primaries$\times$ 8 KHz / 5) for minimum bias Pb–Pb running. The results can be seen in Tables A.6 and A.7 for both sides of the TPC.

To scale up to a ten-year run period we multiply the aforementioned results of the fluences per central event with a factor of $3.2 \times 10^{15}$ (80000 primaries$\times$ 8 KHz / 5$\times$ 2.5$\times$ 10$^6$ sec/year$\times$ 10 years). The results are presented in Table C.8 where the range in the values comes from the lower and upper limit of the 4 layers for both sides of the TPC.

### C.1.3 Admixture of $CH_4$ or $N_2$ in the TPC gas.

The ideal gas mixture for a particular TPC varies with the environment in which that TPC will operate. The necessity of having a low diffusion gas has led to the choice of Ne-$CO_2$ as operating gas of the ALICE TPC.

However, this choice has a number of serious consequences for the operation and desigh of the TPC. The most obvious disadvantage is the drastically increased temperature dependence of the drift velocity as compared to Ar-$CH_4$. Moreover, $CO_2$ is known as a bad quencher, which contradicts the need of a high gas gain to achieve a reasonable signal to noise ratio [156, 157].

Recent investigations [158, 159] have indicated a possible improvement of the above problems. A small admixture of $N_2$ ($\approx 5\%$) as additional quencher increases the stability of the gas mixture significantly without lowering the drift velocity (and gain) to an intolerable extend as increase in the $CO_2$ content would do.

Nitrogen is however sensitive to neutrons. $^{14}$N can capture a thermal neutron to become $^{15}$N which sometimes emits a 10.8 MeV photon. Although this mechanism has a numerous useful applications (detection of explosives, measuring protein contents in living beings) it is not desired in ALICE since the photon can be absorbed by the gas yielding ionisation electrons thus making the TPC sensitive to the background neutron radiation.

To enhance the effect of the admixture, we added 10% $N_2$ in the normal TPC gas (Ne-$CO_2$, 90-10) and did a simulation using the FLUKA transport code. Comparing the lethargy photon spectra, as it is shown in Fig.C.12, with and without the $N_2$ admixture, one can be notice the presence of a 511 keV peak (due to positron annihilation), the 2.2 MeV peak from the neutron capture in Hydrogen and the 7.9 MeV in Copper. In both cases the spectra look similar and there is no sign of the 10.8 MeV photon peak.

However, we should expect a small proton background from the $^{14}$N(n,p)$^{14}$C which is a very important reaction, especially in dosimetry (it contributes substantialy to the person dose from low energy neutrons). For this reason, in FLUKA that reaction is simulated in detail, and each proton is tracked individually. In Fig.C.13 we can see that the (n,p) cross section of $^{14}$N is more than one order of magnitude larger than the (n,$\gamma$). (By the way, that is the same reaction which produces $^{14}$C in the atmosphere, and which is used to date ancient wooden artifacts: plants assimilate $CO_2$ containing

Table C.2: Number of particles per central event (**absorber side**).

| Layers | 1 | 2 | 3 | 4 | Sum |
|---|---|---|---|---|---|
| Protons | 113 | 147 | 134 | 147 | 541 |
| Protons with $E_{\text{kin}} > 10\,\text{MeV}$ | 109 | 144 | 128 | 143 | 524 |
| Electrons | 1097 | 971 | 854 | 954 | 3876 |
| Positrons | 464 | 586 | 334 | 281 | 1665 |
| Photons | 16530 | 34581 | 22930 | 28187 | 102228 |
| Neutrons | 41502 | 49600 | 50853 | 57780 | 199735 |
| Neutrons with $E_{\text{kin}} > 10\,\text{MeV}$ | 3600 | 2700 | 2100 | 2200 | 10600 |
| Muons$^{\pm}$ | 234 | 348 | 368 | 300 | 1250 |
| Pions$^{\pm}$ | 492 | 1449 | 1495 | 1030 | 4466 |
| Pions$^{\pm}$ with $E_{\text{kin}} > 10\,\text{MeV}$ | 492 | 1447 | 1493 | 1029 | 4461 |
| Kaons$^{\pm}$, all with $E_{\text{kin}} > 10\,\text{MeV}$ | 19 | 91 | 72 | 51 | 233 |
| Primaries | 103 | 197 | 567 | 435 | 1302 |
| Charged | 2419 | 3592 | 3257 | 2763 | 12031 |

$^{14}$C while they are alive, and of course stop when they die. From then on, the $^{14}$C they have assimilated starts to decay, and from what is left one can calculate how many years have passed since the plant died.).

Anyway, the proton background from the admixture of 10% $N_2$ in the normal TPC gas, is much smaller compared to that which is expected after the addition of 5% $CH_4$ as it can be seen in Fig.C.11. In case of $CH_4$, prompt neutrons can scatter on hydrogen and produce a significant knockout proton background which is an additional big disadvantage to the ageing effect that it also has [160]. Analyzing one central FLUKA event, it can also be calculated the number of protons that are created in the gas. In case of 10% $N_2$, we have a factor of 2 more produced protons and each of them deposit on average ∼0.85 MeV in a 2 cm track length (about 200 mips in one pad). With the addition of 5% $CH_4$ in the normal TPC gas, we have a factor of 10 more produced protons in the gas.

Table C.3: Number of particles per central event (**non-absorber side**).

| Layers | 1 | 2 | 3 | 4 | Sum |
|---|---|---|---|---|---|
| Protons | 292 | 200 | 155 | 156 | 803 |
| Protons with $E_{\mathrm{kin}} > 10\,\mathrm{MeV}$ | 289 | 198 | 151 | 151 | 789 |
| Electrons | 4476 | 1551 | 1070 | 584 | 7681 |
| Positrons | 1897 | 906 | 339 | 309 | 3451 |
| Photons | 58286 | 60649 | 29010 | 67192 | 215137 |
| Neutrons | 17796 | 35758 | 34999 | 49756 | 138349 |
| Neutrons with $E_{\mathrm{kin}} > 10\,\mathrm{MeV}$ | 1800 | 2000 | 1300 | 1700 | 6800 |
| Muons$^{\pm}$ | 390 | 457 | 368 | 325 | 1540 |
| Pions$^{\pm}$ | 2140 | 1664 | 1452 | 1109 | 6365 |
| Pions$^{\pm}$ with $E_{\mathrm{kin}} > 10\,\mathrm{MeV}$ | 2138 | 1664 | 1451 | 1109 | 6362 |
| Kaons$^{\pm}$, all with $E_{\mathrm{kin}} > 10\,\mathrm{MeV}$ | 164 | 106 | 84 | 53 | 407 |
| Primaries | 85 | 171 | 519 | 474 | 1249 |
| Charged | 9359 | 4884 | 3468 | 2536 | 20247 |

Table C.4: Particle fluences (particles/cm$^2$/primary) per central event (**absorber side**).

| Layers | 1 | 2 | 3 | 4 |
|---|---|---|---|---|
| p | $(1.03\times 10^{-7})\pm 26.7\%$ | $(6.04\times 10^{-8})\pm 6.9\%$ | $(3.93\times 10^{-8})\pm 10.6\%$ | $(4.01\times 10^{-8})\pm 10.6\%$ |
| p with $E_{\text{kin}} > 10\,\text{MeV}$ | $9.96\times 10^{-8}$ | $5.89\times 10^{-8}$ | $3.79\times 10^{-8}$ | $3.88\times 10^{-8}$ |
| $e^{\pm}$ | $(1.01\times 10^{-6})\pm 26.4\%$ | $(6.10\times 10^{-7})\pm 6.8\%$ | $(4.50\times 10^{-7})\pm 26.0\%$ | $(3.16\times 10^{-7})\pm 9.7\%$ |
| n | $(3.42\times 10^{-5})\pm 1.6\%$ | $(2.57\times 10^{-5})\pm 0.3\%$ | $(2.13\times 10^{-5})\pm 0.9\%$ | $(1.85\times 10^{-5})\pm 0.5\%$ |
| n with $E_{\text{kin}} > 10\,\text{MeV}$ | $2.61\times 10^{-6}$ | $1.60\times 10^{-6}$ | $1.05\times 10^{-6}$ | $7.49\times 10^{-7}$ |
| Thermal n | $2.82\times 10^{-6}$ | $2.58\times 10^{-6}$ | $2.44\times 10^{-6}$ | $2.54\times 10^{-6}$ |
| $\gamma$ | $(1.66\times 10^{-5})\pm 10.5\%$ | $(1.31\times 10^{-5})\pm 7.0\%$ | $(1.04\times 10^{-5})\pm 9.1\%$ | $(8.06\times 10^{-6})\pm 15.4\%$ |
| $\mu^{\pm}$ | $(1.47\times 10^{-7})\pm 9.0\%$ | $(1.51\times 10^{-7})\pm 7.3\%$ | $(1.31\times 10^{-7})\pm 13.7\%$ | $(8.22\times 10^{-8})\pm 5.0\%$ |
| $\pi^{\pm}$ | $(2.92\times 10^{-7})\pm 5.7\%$ | $(4.37\times 10^{-7})\pm 3.1\%$ | $(3.71\times 10^{-7})\pm 2.4\%$ | $(2.23\times 10^{-7})\pm 2.8\%$ |
| $\pi^{\pm}$ with $E_{\text{kin}} > 10\,\text{MeV}$ | $2.91\times 10^{-7}$ | $4.36\times 10^{-7}$ | $3.71\times 10^{-7}$ | $2.23\times 10^{-7}$ |
| $k^{\pm}$ with $E_{\text{kin}} > 10\,\text{MeV}$ | $(7.54\times 10^{-9})\pm 14.0\%$ | $(2.37\times 10^{-8})\pm 15.1\%$ | $(1.59\times 10^{-8})\pm 12.5\%$ | $(9.85\times 10^{-9})\pm 27.9\%$ |
| Charged | $(1.55\times 10^{-6})\pm 17.3\%$ | $(1.28\times 10^{-6})\pm 3.6\%$ | $(1.01\times 10^{-6})\pm 12.5\%$ | $(6.72\times 10^{-7})\pm 5.3\%$ |

Table C.5: Particle fluences (particles/cm$^2$/primary) per central event (**non-absorber side**).

| Layers | 1 | 2 | 3 | 4 |
|---|---|---|---|---|
| p | $(1.52\times 10^{-7})\pm 9.6\%$ | $(7.22\times 10^{-8})\pm 11.5\%$ | $(6.34\times 10^{-8})\pm 19.3\%$ | $(3.61\times 10^{-8})\pm 8.5\%$ |
| p with $E_{\text{kin}} > 10\,\text{MeV}$ | $1.50\times 10^{-7}$ | $7.10\times 10^{-8}$ | $6.18\times 10^{-8}$ | $3.54\times 10^{-8}$ |
| $e^{\pm}$ | $(3.50\times 10^{-6})\pm 23.0\%$ | $(1.10\times 10^{-6})\pm 25.1\%$ | $(4.61\times 10^{-7})\pm 15.5\%$ | $(3.08\times 10^{-7})\pm 7.3\%$ |
| n | $(1.27\times 10^{-5})\pm 1.3\%$ | $(1.28\times 10^{-5})\pm 2.1\%$ | $(1.27\times 10^{-5})\pm 1.2\%$ | $(1.27\times 10^{-5})\pm 1.3\%$ |
| n with $E_{\text{kin}} > 10\,\text{MeV}$ | $8.70\times 10^{-7}$ | $5.80\times 10^{-7}$ | $4.47\times 10^{-7}$ | $3.56\times 10^{-7}$ |
| Thermal n | $1.87\times 10^{-6}$ | $1.75\times 10^{-6}$ | $1.77\times 10^{-6}$ | $1.86\times 10^{-6}$ |
| $\gamma$ | $(4.59\times 10^{-5})\pm 11.7\%$ | $(2.91\times 10^{-5})\pm 13.8\%$ | $(1.46\times 10^{-5})\pm 6.5\%$ | $(1.09\times 10^{-5})\pm 15.6\%$ |
| $\mu^{\pm}$ | $(2.81\times 10^{-7})\pm 12.4\%$ | $(2.14\times 10^{-7})\pm 2.2\%$ | $(1.45\times 10^{-7})\pm 8.6\%$ | $(1.06\times 10^{-7})\pm 7.1\%$ |
| $\pi^{\pm}$ | $(8.94\times 10^{-7})\pm 1.0\%$ | $(5.13\times 10^{-7})\pm 2.5\%$ | $(3.65\times 10^{-7})\pm 4.0\%$ | $(2.42\times 10^{-7})\pm 3.0\%$ |
| $\pi^{\pm}$ with $E_{\text{kin}} > 10\,\text{MeV}$ | $8.93\times 10^{-7}$ | $5.11\times 10^{-7}$ | $3.64\times 10^{-7}$ | $2.42\times 10^{-7}$ |
| $k^{\pm}$ with $E_{\text{kin}} > 10\,\text{MeV}$ | $(6.03\times 10^{-8})\pm 3.5\%$ | $(2.80\times 10^{-8})\pm 13.3\%$ | $(1.83\times 10^{-8})\pm 9.3\%$ | $(1.02\times 10^{-8})\pm 6.9\%$ |
| Charged | $(4.89\times 10^{-6})\pm 17.0\%$ | $(1.92\times 10^{-6})\pm 14.3\%$ | $(1.05\times 10^{-6})\pm 7.3\%$ | $(7.03\times 10^{-7})\pm 2.2\%$ |

Table C.6: Particle fluxes (particles/cm$^2$/s) for minimum bias Pb–Pb running (**absorber side**). Same errors with their respective fluences in accordance with a previous table.

| Layers | 1 | 2 | 3 | 4 |
|---|---|---|---|---|
| Neutron Flux [cm$^{-2}$s$^{-1}$] | 4377.6 | 3289.6 | 2726.4 | 2368 |
| Neutron Flux [cm$^{-2}$s$^{-1}$] with $E_{\mathrm{kin}} > 10\,\mathrm{MeV}$ | 334.1 | 204.8 | 134.4 | 95.9 |
| Proton Flux [cm$^{-2}$s$^{-1}$] | 13.2 | 7.7 | 5.0 | 5.1 |
| Proton Flux [cm$^{-2}$s$^{-1}$] with $E_{\mathrm{kin}} > 10\,\mathrm{MeV}$ | 12.7 | 7.5 | 4.9 | 5.0 |
| Pion$^{\pm}$ Flux [cm$^{-2}$s$^{-1}$] | 37.4 | 55.9 | 47.5 | 28.5 |
| Pion$^{\pm}$ Flux [cm$^{-2}$s$^{-1}$] with $E_{\mathrm{kin}} > 10\,\mathrm{MeV}$ | 37.2 | 55.8 | 47.5 | 28.5 |
| Kaon$^{\pm}$ Flux [cm$^{-2}$s$^{-1}$], all with $E_{\mathrm{kin}} > 10\,\mathrm{MeV}$ | 1.0 | 3.0 | 2.0 | 1.3 |

Table C.7: Particle fluxes (particles/cm$^2$/s) for minimum bias Pb–Pb running (**non-absorber side**). Same errors with their respective fluences in accordance with a previous table.

| Layers | 1 | 2 | 3 | 4 |
|---|---|---|---|---|
| Neutron Flux [cm$^{-2}$s$^{-1}$] | 1625.6 | 1638.4 | 1625.6 | 1625.6 |
| Neutron Flux [cm$^{-2}$s$^{-1}$] with $E_{\mathrm{kin}} > 10\,\mathrm{MeV}$ | 111.4 | 74.2 | 57.2 | 45.6 |
| Proton Flux [cm$^{-2}$s$^{-1}$] | 19.5 | 9.2 | 8.1 | 4.6 |
| Proton Flux [cm$^{-2}$s$^{-1}$] with $E_{\mathrm{kin}} > 10\,\mathrm{MeV}$ | 19.2 | 9.1 | 7.9 | 4.5 |
| Pion$^{\pm}$ Flux [cm$^{-2}$s$^{-1}$] | 114.4 | 65.7 | 46.7 | 31.0 |
| Pion$^{\pm}$ Flux [cm$^{-2}$s$^{-1}$] with $E_{\mathrm{kin}} > 10\,\mathrm{MeV}$ | 114.3 | 65.4 | 46.6 | 31.0 |
| Kaon$^{\pm}$ Flux [cm$^{-2}$s$^{-1}$], all with $E_{\mathrm{kin}} > 10\,\mathrm{MeV}$ | 7.7 | 3.6 | 2.3 | 1.3 |

Table C.8: Particle fluences and total absorbed doses per 10 ALICE years.

| Scoring region of TPC electronics | Absorber side | Non-absorber side |
|---|---|---|
| Neutron Fluence [$cm^{-2}$] | (0.6-1.1)$\times 10^{11}$ | 0.4$\times 10^{11}$ |
| Neutron Fluence [$cm^{-2}$] with $E_{kin} > 10$ MeV | (2.4-8.4)$\times 10^{9}$ | (1.1-2.8)$\times 10^{9}$ |
| Proton Fluence [$cm^{-2}$] with $E_{kin} > 10$ MeV | (1.2-3.2)$\times 10^{8}$ | (1.1-4.8)$\times 10^{8}$ |
| Pion Fluence [$cm^{-2}$] with $E_{kin} > 10$ MeV | (0.7-1.4)$\times 10^{9}$ | (0.8-2.9)$\times 10^{9}$ |
| Kaon Fluence [$cm^{-2}$] with $E_{kin} > 10$ MeV | (2.4-7.6)$\times 10^{7}$ | (3.3-19.3)$\times 10^{7}$ |
| Total Dose [Gy] | (0.8-2.5)$\times 10^{0}$ | (0.3-5.7)$\times 10^{0}$ |

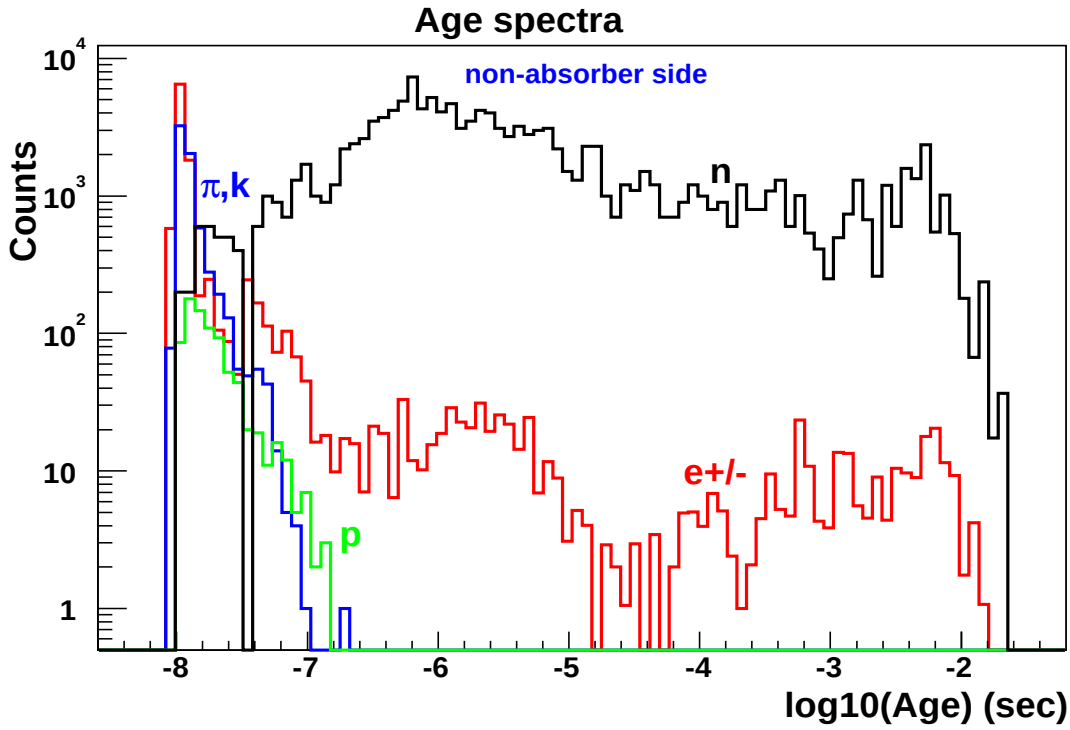


Figure C.2: Age spectra of neutrons, electrons and positrons, pions and kaons, protons in the non-absorber side (one central event).

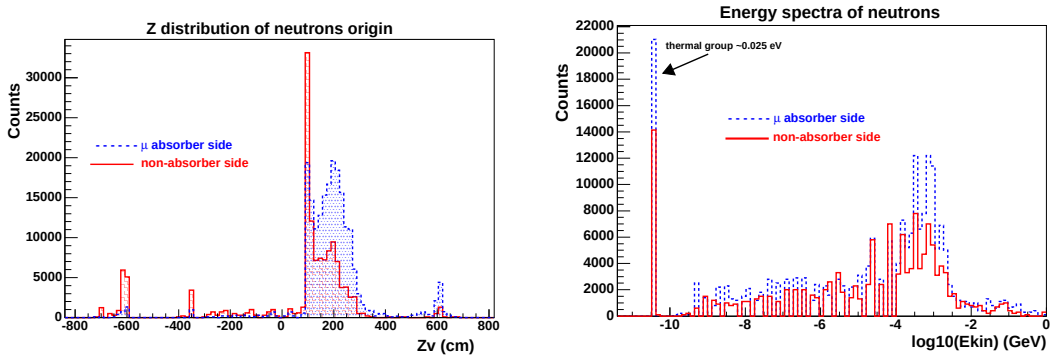


Figure C.3: Z distribution and kinetic energy of neutrons in the absorber side (dashed line) and non-absorber side (solid line) of the TPC respectively (one central event).

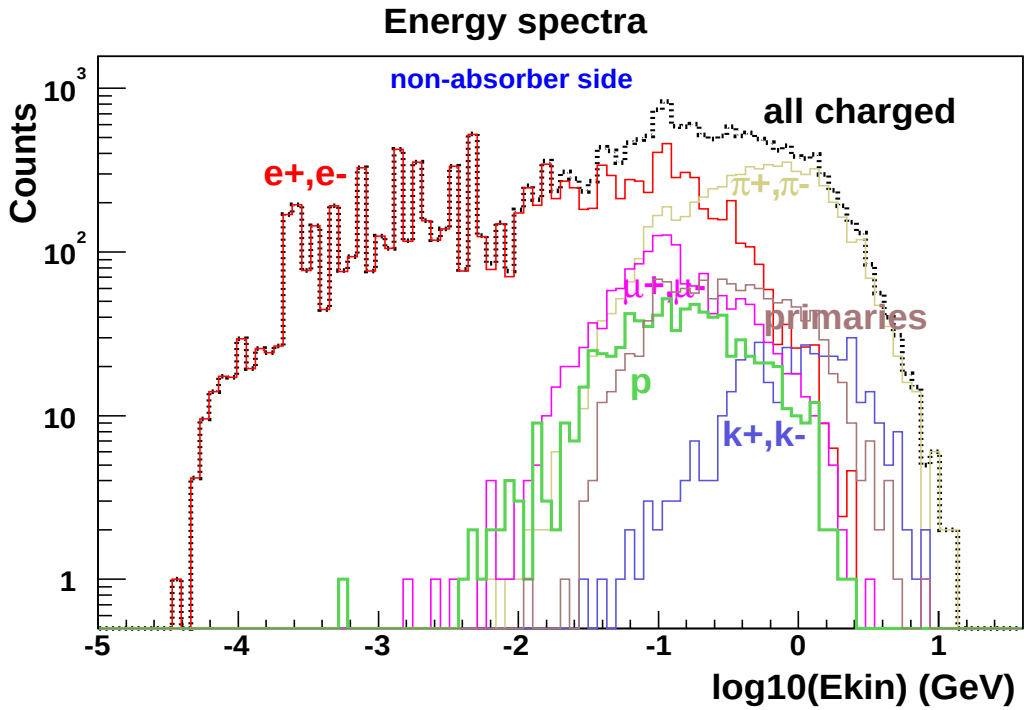


Figure C.4: Energy spectra of all charged particles in the non-absorber side (one central event).

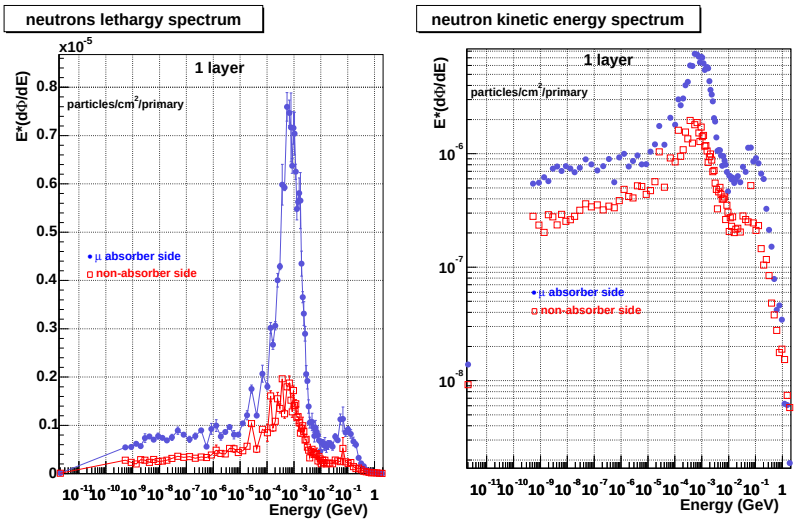


Figure C.5: Lethargy and kinetic energy spectra of neutrons in the absorber side (full circles) and non-absorber side (empty rectangles) of the TPC respectively (one central event).

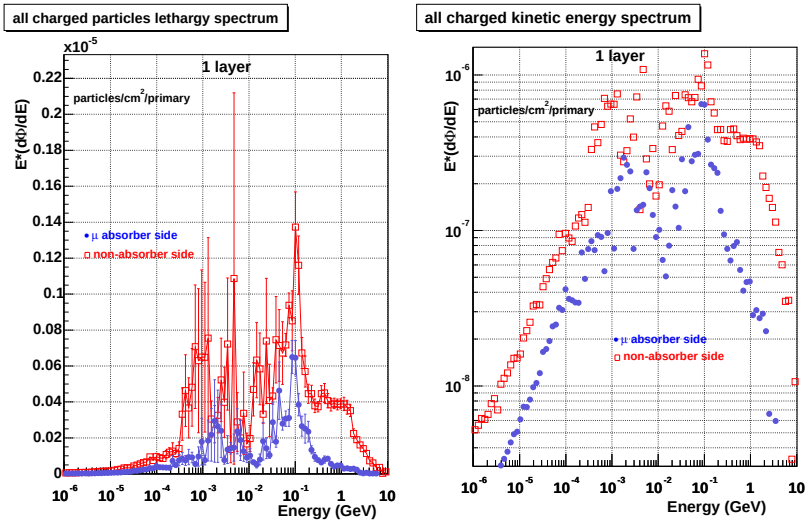


Figure C.6: Lethargy and kinetic energy spectra of all charged particles in the absorber side (full circles) and non-absorber side (empty rectangles) of the TPC respectively (one central event).

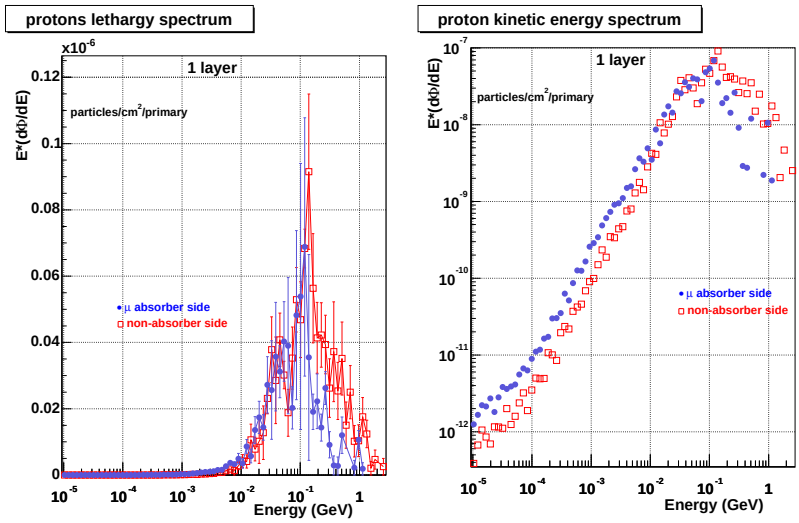


Figure C.7: Lethargy and kinetic energy spectra of protons in the absorber side (full circles) and non-absorber side (empty rectangles) of the TPC respectively (one central event).

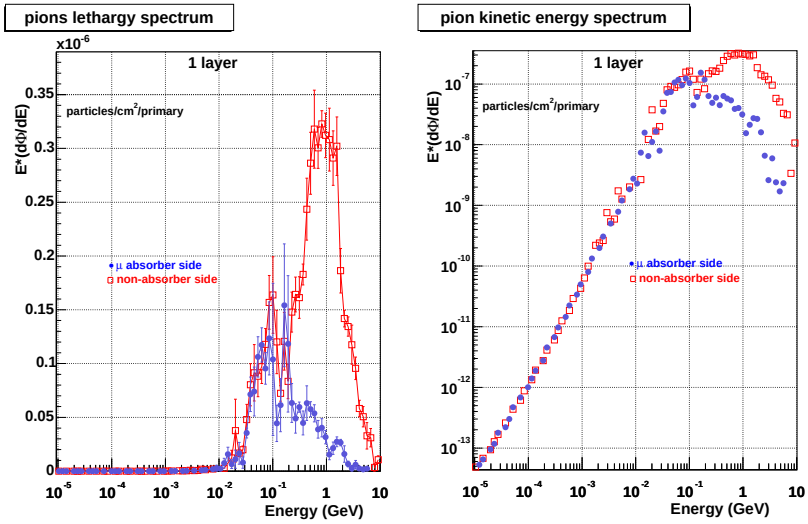


Figure C.8: Lethargy and kinetic energy spectra of all pions particles in the absorber side (full circles) and non-absorber side (empty rectangles) of the TPC respectively (one central event).

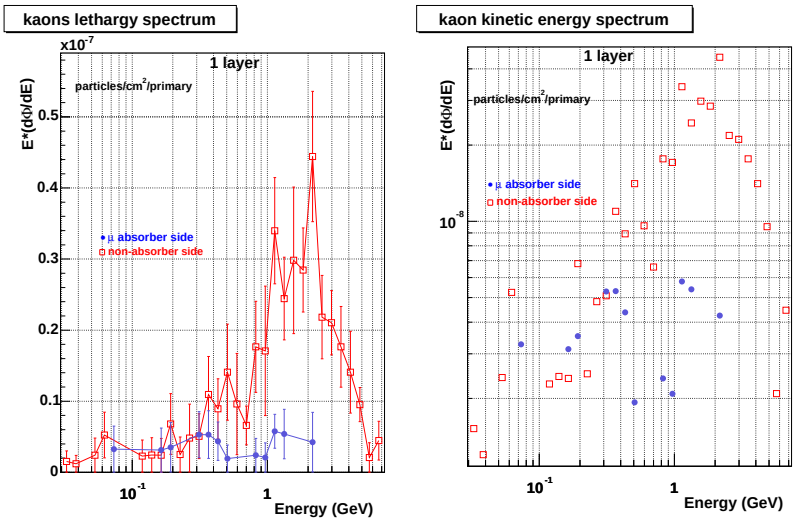


Figure C.9: Lethargy and kinetic energy spectra of kaons in the absorber side (full circles) and non-absorber side (empty rectangles) of the TPC respectively (one central event).

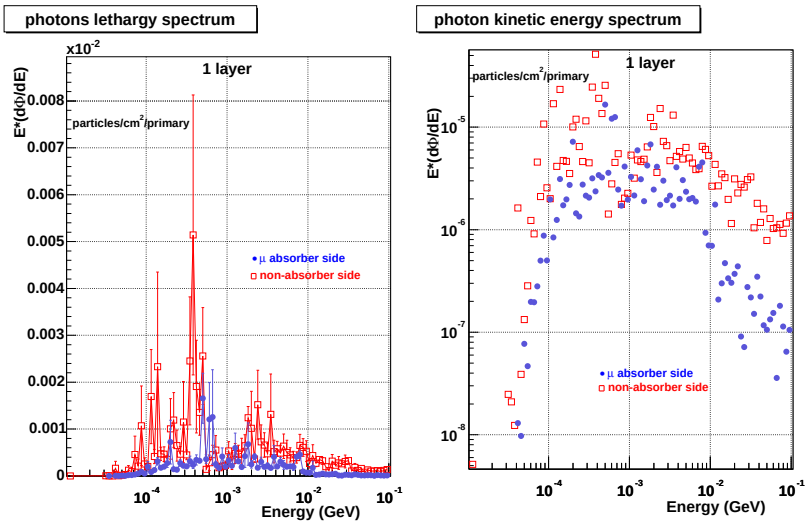


Figure C.10: Lethargy and kinetic energy spectra of all photons particles in the absorber side (full circles) and non-absorber side (empty rectangles) of the TPC respectively (one central event).

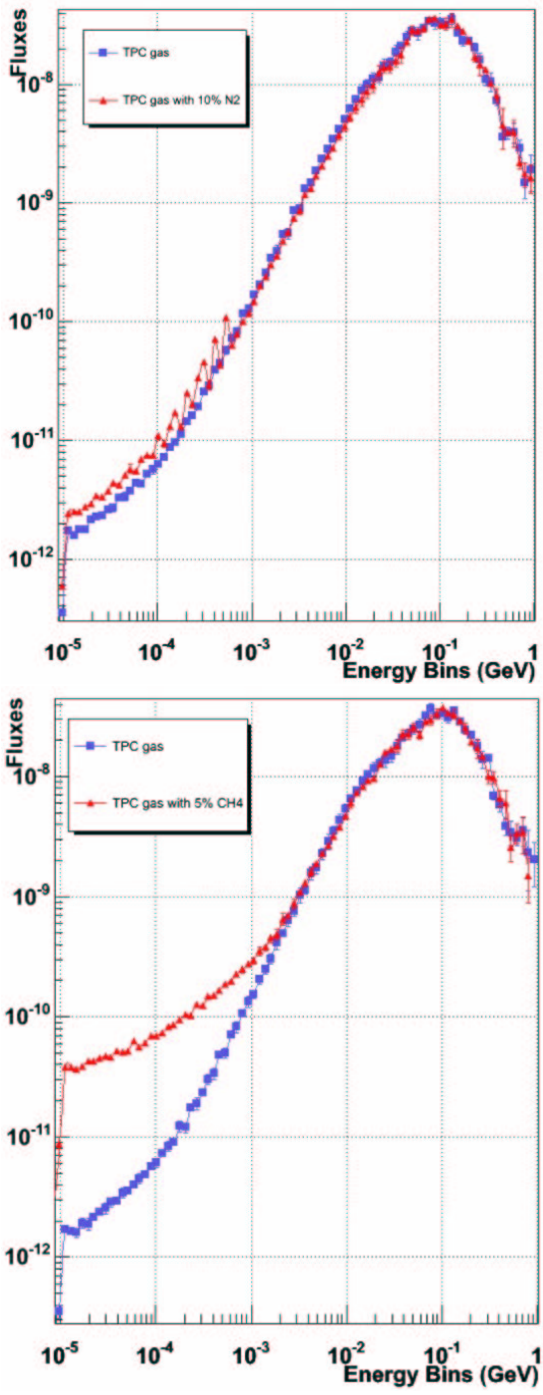


Figure C.11: Kinetic spectra of protons in the normal TPC gas (blue rectangles) and after the addition of 10% $N_2$ or 5% $CH_4$ respectively (red triangles).

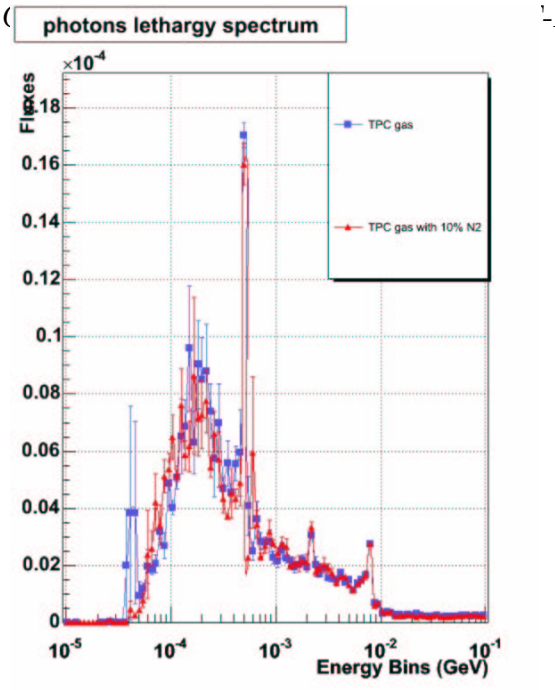


Figure C.12: Lethargy spectra of photons in the normal TPC gas (blue rectangles) and after the addition of 10% $N_2$ respectively (red triangles).

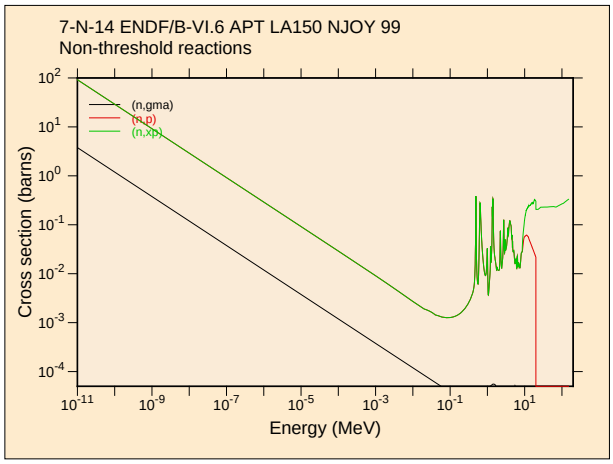


Figure C.13: (n,p) and (n,$\gamma$) cross sections of $^{14}$N.

# Bibliography


[1] B. Müller, *Physics of the Quark Gluon Plasma* `nucl-th/9211010` (1992).

[2] K.G. Wilson, Phys. Rev. **D10** (1974) 2445.

[3] A. Andronic and P. Braun-Munzinger, *Ultrarelativistic nucleus-nucleus collisions and the quark-gluon plasma*, VIII Hispalensis International Summer School, Oromana (Seville, Spain), June 9-21, 2003, `hep-ph/0402291` (2004).

[4] F. Karsch and E. Laermann *Thermodynamics and in-medium hadron properties from lattice QCD*, `hep-lat/0305025` (2003).

[5] See e.g. H. Satz, Nucl. Phys. **A715** (2003) 3, `hep-ph/0209181`.

[6] `http://www.bnl.gov/RHIC`

[7] G.D. Westfall, *et al.*, Phys. Rev. Lett. **37** (1976) 1202.

[8] J.D. Bjorken, Phys. Rev. D 27 (1983) 140.

[9] K. Kajantie, L. McLerran, Ann. Rev. Nucl. Part. Sci. 37 (1987) 293. J.W. Harris, B. Müller, Ann. Rev. Nucl. Part. Sci. 46 (1996) 71 [hep-ph/9602235]; S.A. Bass, M. Gyulassy, H. Stöcker, and W. Greiner, J. Phys. G25 (1999) R1 [hep-ph/9810281].

[10] T. Peitzmann and M.H. Thoma, Phys. Rep. 364 (2002) 175 [hep-ph/0111114].

[11] R. Rapp, J. Wambach, Adv. Nucl. Phys. 25 (2000) 1 [hep-ph/9909229]; J.P. Wessels et al. (CERES), Nucl. Phys. A 715 (262c) 2003, [nucl-ex/0212015] and ref. therein.

[12] J. Rafelski, Nucl. Phys. **A418** 215c (1984).

[13] J. Rafelski, J. Letessier, J. Phys. G 30 (2004) S1 [hep-ph/0305284]; R. Stock, hep-ph/0312039.

[14] H. Satz, Rep. Prog. Phys. 63 (2000) 1511 [hep-ph/0007069].

[15] S.S. Adler et al. (PHENIX), Phys. Rev. Lett. 91 (2003) 072301 [nucl-ex/0304022], Phys. Rev. Lett. 91 (2003) 072303 [nucl-ex/0306021], nucl-ex/0308006; J. Adams et al. (STAR), Phys. Rev. Lett. 91 (2003) 172302 [nucl-ex/0305015], Phys. Rev. Lett. 91 (2003) 072304 [nucl-ex/0306024]; B.B. Back et al. (PHOBOS), Phys. Rev. Lett. 91 (2003) 072302 [nucl-ex/0306025]; I. Arsene et al. (BRAHMS), Phys. Rev. Lett. 91 (2003) 072305 [nucl-ex/0307003]; G. Agakichiev et al. (CERES), Phys. Rev. Lett. 92 (2004) 032301 [nucl-ex/0303014].

[16] M. Asakawa, U. Heinz, B. Müller, Phys. Rev. Lett. 85 (2000) 2072 [hep-ph/0003169]; S. Jeon, V. Koch, Phys. Rev. Lett. 85 (2000) 2076 [hep-ph/0003168].

[17] M. Gyulassy and M Plümer, Phys. Lett. **B243** (1990) 432.

[18] X.N. Wang and M. Gyulassy, Phys. Rev. Lett. **68** (1992) 1480.

[19] U. Heinz, *Concepts of Heavy-Ion Physics*, CERN-2004-001, pp.127-178, `hep-ph/0407360` (2004)

[20] S. Hands *The Phase Diagram of QCD*, `physics/0105022` (2001)

[21] Z. Fodor, S.D. Katz, J. High Ener. Phys. 404 50, `hep-lat/0402006` (2004).

[22] updated version of Figure in P. Braun-Munzinger, J. Stachel, J. Phys. G 28 1971 (2002), taken from A. Andronic, P. Braun-Munzinger, J. Stachel, to be published.

[23] J. Stachel *Has the Quark Gluon Plasma been seen?*, `nucl-ex/0510077` (2005).

[24] M. Stephanov *QCD phase diagram and the critical point*, `hep-ph/0402115` (2005).

[25] S. Jeon, V. Koch, *Event-by-Event Fluctuations*, review for "Quark-Gluon Plasma 3", eds. R.C. Hwa and X.-N. Wang, World Scientific, Singapore, `hep-ph/0304012`, (2003).

[26] M.A. Stephanov, K. Rajagopal, and E.V. Shuryak, Phys. Rev. Lett. 81 (1998) 4816.

[27] G. Agakichiev, *et al.*, (CERES Collaboration), Eur. Phys. J. **C4** (1998) 231. G. Agakichiev, *et al.*, (CERES Collaboration), Eur. Phys. J. **C4** (1998) 249.

[28] G. Agakichiev et al. (CERES), Phys. Rev. Lett. 75 (1995) 1272 and `nucl-ex/0506002`.

[29] A. Marin, *et al.*, (CERES Collaboration), Nucl. Phys. **A661** (1999)

[30] D. Miśkowiec (CERES Collaboration), *Recent Results from CERES*, Proceedings of Quark Matter 2005, Budapest, in print.

[31] J. Seguinot and T. Ypsilantis, Nucl. Instr. Meth. **1977** (142) .

[32] J. Slivova, *"Azimuthal Correlations of High-$p_T$ Pions in 158 A·GeV/c Pb-Au Collisions Measured by the CERES Experiment"*, PhD thesis, University of Heidelberg, 2003.

[33] W. R. Leo, *Techniques for Nuclear and Particle Physics Experiments*, Springer-Verlag, 1993.

[34] H. Tilsner, *"Two-particle Correlations at 40, 80, and 158 A·GeV/c Pb-Au Collisions Measured by the CERES Experiment"*, PhD thesis, University of Heidelberg, 2002.

[35] M. Stephanov, K. Rajagopal, and E. Shuryak, Phys. Rev. **D60** (1999) 14028.

[36] M. Gazdzicki and S. Mrowczynski, Z. Phys. **C54** (1992) 127.

[37] S. Voloshin, V. Koch, and H. Ritter, Phys. Rev. **C60** (1999) 024901.

[38] S. Voloshin, *Mean $p_T$ fluctuations from 2- and 4-particle correlations.*, `nucl-th/0206052` (2002).

[39] T.A. Trainor, *Event-by-Event Analysis and the Central Limit Theorem*, `hep-ph/0001148` (2000).

[40] R. L. Ray *et al.* (STAR Collaboration), Nucl. Phys. **A715** (2003) 45.

[41] C. Pruneau, S. Gavin, and S. Voloshin, Phys. Rev. **C66** (2002) 044904.

[42] A. Bialas, and M. Gazdzicki, Phys. Lett. **B252** (1990) 483.

[43] NA49 Collaboration, *Transverse Momentum Fluctuations at 158 A·GeV/c*, `hep-ph/0001148` (2000).

[44] NA49 Collaboration, *Transverse Momentum Fluctuations in nuclear collisions at 158 A·GeV/c*, Phys. Rev. **C70** (2004) 034902.

[45] H. Appelshäuser *et al.* (CERES Collaboration), Nucl. Phys. **A727** (2003) 97, `nucl-ex/0305002` (2000).

[46] H. Sako and H. Appelshäuser for the CERES Collaboration, *Event-by-event fluctuations in 40, 80, and 158 A·GeV/c Pb+Au collisions*, (Quark Matter 04, Proc. Int. Conf. on Ultra-Relativistic Nucleus-Nucleus Collisions, Oakland, 2004) J. Phys. G 30 (2004) S1371-1375, nucl-ex/0403037, preprint.

[47] M. Tannenbaum, Phys. Lett. **B498** (2001) 29.

[48] P. Braun-Munzinger *et al.*, Nucl. Phys. **A697** (2002) 902.

[49] STAR Collaboration, S. Voloshin *et al.*, `nucl-ex/0109006` (2001).

[50] STAR Collaboration, J. Adams *et al.*, `nucl-ex/0308033` (2003).

[51] PHENIX Collaboration, S. Adler *et al.*, `nucl-ex/0310005` (2003).

[52] M. Stephanov, Phys. Rev. **D65** (2002) 096008.

[53] K. Braune, et al., Phys. Lett. **B123** (1983) 467.

[54] WA98 Collaboration, M.M. Aggarwal, *et al.*, Eur. Phys. J. **C18** (2001) 651.

[55] CERES Collaboration, D. Miśkowiec, *et al.*, in *Proccedings of the International Workshop XXX on Gross Properties of Nuclei and Nuclear Excitations*, Hirschegg, Austria, January 13-19, 2002.

[56] WA97 Collaboration, W. Andersen, *et al.*, Phys. Lett. **B449** (1999) 401.

[57] H. Appelshäuser *et al.* (CERES Collaboration), J. Phys. G: Nucl. Part. Phys. **30** (2004) S1376.

[58] NA49 Collaboration, T. Anticic *et al.*, `hep-ex/0311009` (2000).

[59] G.D. Westfall *et al.* (STAR Collaboration), J. Phys. G: Nucl. Part. Phys. **30** (2004) S1389.

[60] S. Gavin, J. Phys. G: Nucl. Part. Phys. **30** (2004) S1385.

[61] S. Gavin, Phys. Rev. Lett. **92** (2004) 162301.

[62] E.G. Ferreiro, J. Phys. G: Nucl. Part. Phys. **30** (2004) S1159.

[63] E.G. Ferreiro, F. del Moral and C. Pajares, Phys. Rev. **C69** (2004) 034901.

[64] D. Miśkowiec and D. Antończyk, *Centrality calibration of the CERES' 2000 data*, CERES note, January 31, 2005

[65] O. Busch, *Track Fitting in the CERES TPC*, CERES note, March 29, 2005

[66] K.J. Eskola, K. Kajantie, J. Lindfors, Nucl. Phys. **B323** (1989) 37, for implementation see `http://www.gsi.de/~misko/overlap`.

[67] C. Pruneau (STAR Collaboration),*Excitation Function of mean $p_T$ and Net Charge Fluctuations at RHIC*, Proceedings of Quark Matter 2004, Oakland, `nucl-ex/0401016`.

[68] A.M. Poskanzer and S. Voloshin, *Methods of analyzing anisotropic flow in relativistic nuclear collisions*, Phys. Rev. **C58** (1998) 1671.

[69] C. Adlair, Phys. Rev. Lett. 90 (2003) 032301.

[70] C. Adlair, Phys. Rev. Lett. 90 (2003) 082302.

[71] J. Milošević (CERES Collaboration),*Strange and charged particle elliptic flow in Pb-Au collisions at 158 GeV*, Proceedings of Quark Matter 2005, Budapest, in print.

[72] J. Milošević, private communication.

[73] D. Miśkowiec, private communication.

[74] H. Appelshäuser, private communication.

[75] G. Agakichiev et al. (CERES), Phys. Rev. Lett. 92 (2004) 032301.

[76] C. Garabatos, F. Hahn, G. Tsiledakis and A. Wasem, *TRD gas regeneration by cryogenic distillation* , ALICE Internal NOTE 37-2002 (2002).

[77] A.Andronic et al., Nucl. Instr. Meth. Phys. Res. A **498** (2003) 143.

[78] O. Kiselev et al., Nucl. Instr. Meth. Phys. Res. A **367** (1995) 306.

[79] U. Becker et al., Nucl. Instr. Meth. Phys. Res. A **306** (1991) 194.

[80] Th. Berghofer et al., Nucl. Instr. Meth. Phys. Res. A **525** (2004) 544.

[81] P. Bernardini et al., Nucl. Instr. Meth. Phys. Res. A **355** (1995) 428.

[82] U. von Hagel et al., Nucl. Instr. Meth. Phys. Res. A **420** (1999) 429.

[83] E. Oettinger et al., Nucl. Instr. Meth. Phys. Res. A **412** (1998) 355.

[84] W. Walkowiak et al., Nucl. Instr. Meth. Phys. Res. A **449** (2000) 299.

[85] *ALICE TRD Technical Design Report*, CERN/LHCC 2001-021, October 2001; *http://www-alice.gsi.de/trd/trd*.

[86] T. Mahmoud, *"Development of the Readout Chambers of the Alice TRD and evaluation of its physics performance in the quarkonium sector"*, PhD thesis, University of Heidelberg, 2004.

[87] L.G. Christophorou et al, Nucl. Instr. Meth. **171** (1980) 491.

[88] B. Dolgoshein et al., Nucl. Instr. Meth. Phys. Res. A **294** (1990) 473.

[89] T. Kunst, B. Götz and B. Schmidt, Nucl. Instr. Meth. Phys. Res. A **324** (1993) 127.

[90] U. Becker et al., Nucl. Instr. Meth. Phys. Res. A **421** (1999) 54; *http://cyclo.mit.edu/drift/www*.

[91] R. Veenhof, Nucl. Instr. Meth. Phys. Res. A **419** (1998) 726; *http://consult.cern.ch/writeup/garfield/*.

[92] F. Sauli, CERN Yellow Report 77-09 (1977).

[93] S.F. Biagi, Nucl. Instr. Meth. Phys. Res. A **421** (1999) 234. Magboltz 2, version 5.3, is available from the author (sfb@hep.ph.liv.ac.uk).

[94] W.H. Miller and H. Morgner, J. Chem. Phys. 67, 4923 (1977).kis

[95] J.E. Velazco, J.H. Kolts, and D.W. Setser, J. Chem. Phys. 69, 4357 (1978).

[96] P. Cwetanski, Proc. IEEE Nuclear Science Symposium and Medical Imaging Conference, Lyon, France, Oct. 2000, 5/39-43.

[97] B.R. Bulos and A.V.Phelps, Phys. Rev. A14, 615 (1976).

[98] Y.Nakamura, Aust. J. Phys. 48, 357 (1995).

[99] A.Andronic, S.Biagi, P.Braun-Munzinger, C.Garabatos and G.Tsiledakis, Nucl. Instr. Meth. Phys. Res. A **523** (2004) 302.

[100] A. Ferrari, J. Ranft and P.R. Sala, "The FLUKA radiation transport code and its use for space problems", Physica Medica, **XVII**, Suppl. 1, 72-80 (2001)

A. Fassò, A. Ferrari, J. Ranft and P.R. Sala, "FLUKA: Status and Prospective for Hadronic Applications", Proceedings of the MonteCarlo 2000 Conference, Lisbon, October 23–26 2000, A.Kling, F.Barao, M.Nakagawa, L.Tavora, P.Vaz - eds. , Springer-Verlag Berlin, p.955-960 (2001).

A. Fassò, A. Ferrari, P.R. Sala, "Electron-photon transport in FLUKA: status", Proceedings of the MonteCarlo 2000 Conference, Lisbon, October 23–26 2000, A.Kling, F.Barao, M.Nakagawa, L.Tavora, P.Vaz - eds., Springer-Verlag Berlin, p.159-164 (2001)

[101] `http://www.fluka.org/`

[102] A. Capella and J. Tran Thanh Van, Phys. Lett. 93B, 146 (1980)

[103] K. Hänssgen and J. Ranft, *The Monte Carlo code* NUCRIN *to simulate inelastic hadron–nucleus interactions below 5 GeV*, Comp. Phys. Comm. 39, 53–70 (1986)

[104] A. Ferrari and P.R. Sala, *A new model for hadronic interactions at intermediate energies for the* FLUKA *code*, Proc. of the MC93 International Conference on Monte Carlo Simulation in High Energy and

Nuclear Physics, Tallahassee, Florida, 22–26 February 1993. Edited by P. Dragovitsch, S.L. Linn, M. Burbank, World Scientific, p 277–288, Singapore (1994).

[105] A. Ferrari, J. Ranft, P.R. Sala and S. Roesler, *Cascade particles, nuclear evaporation and residual nuclei in high-energy hadron-nucleus interactions*, Z. Phys. C70, 413 (1996)

[106] A. Ferrari, J. Ranft, P.R. Sala and S. Roesler, *The production of residual nuclei in peripheral high-energy nucleus-nucleus*, Z. Phys. C71, 75 (1996)

[107] P.A. Aarnio,A. Fassò, A. Ferrari,H.-J. Möhring, J. Ranft, P.R. Sala, G.R. Stevenson and J.M. Zazula, FLUKA *: Hadronic Benchmarks and Applications*, Proc. of the MC93 International Conference on Monte Carlo Simulation in High Energy and Nuclear Physics, Tallahassee, Florida, 22–26 February 1993. (P. Dragovitsch, S.L. Linn, M. Burbank, Eds.), World Scientific, p 88, Singapore (1994).

[108] A. Ferrari,T. Rancati and P.R. Sala, FLUKA *Applications in High-Energy Problems: From LHC to ICARUS and Atmospheric Showers*, Proc. of The Third Workshop on Simulating Accelerator Radiation Environments (SARE-3), KEK, Tsukuba, Japan, p.165 (1997).

[109] C. Birattati, E. De Ponti, A. Esposito, A. Ferrari, M. Pelliccioni and M. Silari, *Measurements and characterization of high-energy neutron fields*, Nucl. Instr. Meth. A338, 534, (1994).

[110] A. Ferrari, P.R. Sala, R. Guaraldi and F. Padoani, *An improved multiple scattering model for charged particle transport*, Nucl. Instr. Meth. B71, 412, (1992).

[111] A. Morsch and B. Pastircak, *Radiation in ALICE Detectors and Electronics Racks*, ALICE Internal NOTE 28-2002 (2002)

[112] *A Transition Radiation Detector for Electron Identification with the ALICE Central Detector*. Addendum to ALICE Proposal, CERN/LHCC 99-13, LHCC/P3-Addendum 2, 7 May 1999.

[113] *"Transition Radiation Detector"* ALICE Technical Design Report, CERN/LHCC 2001-021 (2001).

[114] M.N. Mazziotta, *A Monte Carlo code for full simulation of a transition radiation detector*, Comp. Phys. Comm. 132, 110 (2000).

[115] A. Andronic et al., *Prototype tests for the ALICE TRD*, Presented at the IEEE Nuclear Science Symposium and Medical Imaging Conference, Lyon, France, 15–20 Oct. 2000, ALICE-PUB-2000-034 (2001).

[116] O. Busch et al., Nucl. Instr. Meth. Phys. Res. A **525** (2004) 153.

[117] A.Andronic et al., Nucl. Instr. Meth. Phys. Res. A **522** (2004) 40.

[118] E. Cuccoli, A. Ferrari and G.C. Panini, *A group library from JEF 1.1 for flux calculations in the LHC machine detectors*, JEF-DOC-340 (91) (1991)
`http://www.slac.stanford.edu/esh/rp/docs/FLUKA/papers/⇝ bibliography.html`.

[119] `http://www.nea.fr/html/databank/`

[120] `http://www-rsicc.ornl.gov/rsic.html`

[121] `http://www-nds.iaea.or.at/`

[122] `http://http://t2.lanl.gov/codes/`

[123] `http://www.nndc.bnl.gov/nndc/nudat/`

[124] K.J.R. Rosman and P.D.P. Taylor, *Isotopic composition of the elements 1997*, J. Phys. Chem. Ref. Data 27, 1275 (1998).

[125] G. Audi and A.H. Wapstra, *The 1995 update to the atomic mass evaluation*, Nucl. Phys. A595, 409 (1995)
`http://wwwndc.tokai.jaeri.go.jp/NuC/index.html`

[126] `http://t2.lanl.gov/cgi-bin/nuclides/endind`

[127] Academic Press, New York

[128] `http://www.nndc.bnl.gov/nndc/ensdf/ensdfindex.html`

[129] L.V. Groshev, L.I. Govor, A.M. Demidov and A.S. Rakhimov, *Spectra of $\gamma$ rays and level schemes of $Xe^{130}$ and $Xe^{132}$ from the reaction (n,$\gamma$)*, Yad. Fiz. 13, 1129 (1971); Sov. J. Nucl. Phys. 13, 647 (1971).

[130] W. Gelletly, W.R. Kane and D.R. MacKenzie, *Neutron-capture gamma rays from the 9.47-eV resonance in* $^{129}Xe(n,\gamma)^{130}Xe$, Phys. Rev. C9, 2363 (1974).

[131] W. Gelletly, W.R. Kane and D.R. MacKenzie, *Neutron-capture gamma rays from the 14.1-eV resonance in* $Xe^{131}(n,\gamma)Xe^{132}$, Phys. Rev. C3, 1678 (1971).

[132] B. Fogelberg and W. Mampe, *Determination of the neutron binding energy of the delayed neutron emitter* $^{137}Xe$, Z. Phys. A281, 89 (1977).

[133] S.G. Prussin, R.G. Lanier, G.L. Struble, L.G. Mann and S.M. Schoenung, *Gamma rays from thermal neutron capture in* $^{136}Xe$, Phys. Rev. C3, 1001 (1977).

[134] M.A. Lone, R.A. Leavitt and D.A. Harrison, *Prompt Gamma Rays from Thermal-Neutron Capture*, Atomic Data and Nuclear Data Tables 26, 511 (1981).

[135] J.K. Tuli, *Thermal neutron capture gamma rays*, `http://www-nds.iaea.or.at/wallet/tnc/capgam.shtml`.

[136] G.L. Molnár, Zs. Révay, T. Belgya and R.B. Firestone, *The new prompt gamma-ray catalogue for PGAA*, Appl. Rad. Isot. 53, 527 (2000).

[137] S.A. Hamada, W.D. Hamilton and B. Moer, *Gamma-gamma directional correlation measurements in* $^{130,132}Xe$ *following neutron capture by natural xenon*, J. Phys. G14, 1237 (1988).

[138] A. Fassò, A. Ferrari, P.R. Sala and G. Tsiledakis, *Implementation of Xenon capture gammas in FLUKA for TRD background calculations* , ALICE Internal NOTE 28-2001 (2001).

[139] A. Morsch, *"ALIFE: A Geometry Editor and Parser for FLUKA"*, ALICE Internal NOTE 29-1998 (1998).

[140] A. Morsch and S. Roesler, *Radiation studies for the ALICE environment using FLUKA and ALIFE*, CERN ALICE/PUB 98-19 (1998).

[141] AliRoot `http://alisoft.cern.ch/offline/`,
Root `http://root.cern.ch/` .

[142] GEANT 3.21 Package, CERN Program Library W5013.

[143] N.van Eijndhoven et al., *The ALICE Event Generator Pool*, ALICE Internal NOTE 95-32 (1995).

[144] N. Rohrig, *Plotting Neutron Fluence Spectra*, Health Physics Vol. 45, No. 3, (September), pp. 817-818 (1983).

[145] G. Tsiledakis, A. Fassò, P. Foka, A. Morsch and A. Sandoval, *Background in the ALICE TRD due to neutron capture in Xe*, ALICE Internal NOTE 10-2003(2003).

[146] S.A. Cetin and A. Romaniouk, *Induced radioactivity in the active gas system of ATLAS-ID-TRT*, ATL-INDET-2002-001 (2002).

[147] *Radiological Health Handbook*, U.S. Department of Health Education and Welfare (1970).

[148] *Caltech Radiation Safety Training and Safety Manual*, `http://www.cco.caltech.edu/~safety/trm.html"`.

[149] *CERN Radiation Safety manual*, (1996)

[150] *ATLAS Inner Detector Technical Design Report*, CERN/LHCC/97-17 (1997)

[151] I. Dawson and C. Buttar *The radiation environment in the ATLAS inner detector*,Nucl. Instr. Meth. A 453, 461-467 (2000)

[152] The ALICE Collaboration, *Technical proposal for a large ion collider experiment at the CERN LHC.* CERN/LHCC/95-71 (1995).

[153] G. Tsiledakis *et al.*, GSI Report 2004, in print.

[154] *Time Projection Chamber* ALICE Technical Design Report, CERN/LHCC/2000-001 (2000).

[155] *The ALICE TPC Front End Electronics*, `http://ep-ed-alice-tpc.web.cern.ch/ep-ed-alice-tpc/`.

[156] R. Veenhof, *Choosing a gas mixture for the ALICE TPC*, ALICE Internal NOTE 29-2003(2003).

[157] H.R. Schmidt, *The LHC Experiment ALICE-TPC Challenges at High Multiplicities*, ALICE Internal NOTE in preparation (2005).

[158] C. Garabatos, *The ALICE TPC*, Nucl. Instr. Meth. A 535, 197-200 (2004).

[159] J. Wiechula *et al High-precision measurement of the electron drift velocity in Ne-$CO_2$*,Nucl. Instr. Meth. A 548, 582-589 (2005).

[160] R.Bouclier et al.,*Results of wire chamber ageing tests with $CH_4$* Nucl. Instr. Meth. Phys. Res. A **346** (1994) 114.

# Curriculum Vitae

## Personal Data

| | |
|---|---|
| Name | Georgios Karolos |
| Surname | Tsiledakis |
| Place of Birth | Bologna (Italy) |
| Date of Birth | 02 November 1972 |
| Marital Status | single |
| Nationality | greek |

## Education

| | |
|---|---|
| 09 / 1982 - 06 / 1990 | Lyceum (Secondary School), Serres, Greece<br>Average grade 18.7 over 20 (excellent) |
| 09 / 1990 - 11 / 2000 | Aristotle University (graduate in Physics), Thessaloniki.<br>Diploma thesis 'Living matter as a detector of weakly interacting particles', supervised by Prof. Zioutas<br>Main subject Particle Physics<br>Average grade 7.3 over 10 (very good) |
| 08 / 2001 - 11 / 2005 | Doctoral fellowship at the Gesellschaft für Schwerionenforschung and preparation of the dissertation |

## Publications

1. *Implementation of Xenon capture gammas in FLUKA for TRD background calculations* , ALICE Internal NOTE 28-2001 (2001)

2. *TRD gas regeneration by cryogenic distillation* , ALICE Internal NOTE 37-2002 (2002)

3. *Background in the ALICE TRD due to neutron capture in Xe*, ALICE Internal NOTE 10-2003 (2003)

4. *Pulse height measurements and electron attachment in drift chambers operated with Xe,$CO_2$ mixtures* Nucl. Instr. Meth. Phys. Res. A498 (2003)

5. *Drift velocity and gain in argon- and xenon-based mixtures*, Nucl. Instrum. Meth. A523 (2004) 302

## Talks

1. *Measurements of electron attachment in Xe, $CO_2$ (15%) gas of ALICE TRD*, DPG Tagung, Tubingen, 2003

2. *Background in the ALICE TRD and in the TPC electronics based on FLUKA calculations*, DPG Tagung, Köln, 2004

3. *Event-by-Event Fluctuations of the Mean Transverse Momentum at SPS Energy*, DPG Tagung, Berlin, 2005

4. *Correlations/fluctuations from SPS*, overview talk, RHIC & AGS Annual Users' Meeting, BNL, USA, 20-24 June, 2005

5. *Scale dependence of Event-by-Event mean $p_T$ fluctuations at top SPS energy*, RNM meeting, GSI, 4 July 2005

6. V-I Workshop on 'Physics of strongly interacting matter at high densities' Bad Liebenzell, 3-5 October 2005 (contents as previous)

# *Acknowledgements*

I am sincerely indebted to my supervisor Prof. Dr. Braun-Munzinger for the opportunity to join his group and work at GSI. He patiently taught me how to think in science, the process to follow in order to do research and to express and understand complicated concepts by means of intuitive examples. I direct many thanks to Prof. Dr. Appelshäuser who has guided me in that complex field of fluctuations and watched over my progress with care and interest. I am also grateful to Prof. Dr. Stachel who has provided many valuable suggestions for improving the work. No word of thanks could ever express what I own to Prof. Dr. Sandoval and to Dr. Foka who supervised a big part of my work here and for being always attentive to my problems and questions. Dr. Andronic, Dr. Garavatos and Dr. Miskowiec, saved the project during its darkest phase...their perceptive suggestions, comments and critiques did wonders for the study and were invaluable. Going far beyond the call of duty, Alberto Fassò commented in detail on the 'FLUKA' part of my thesis and gave me the confidence to attempt a more expansive study. All 'CERES' and 'ALICE' students and scientists of GSI, Heidelberg and CERN deserve a special mention, since they alerted me to themes demanding further attention and helped me to give a formal shape to my studies and fill the gaps of my always incomplete training.

Prof. Zioutas convinced me to abandon the adventurous life I had and invited me at CERN...I wish I could deserve his trust and I will do my best to live up to his high expectations.

To all my friends I apologize because I have not made a lengthy list of all of you, but you know I keep you in my thoughts.

Laetitia, thank you for being so patient and persistent. After so many sad washouts you had being the second priority, you showed me that 'Life must be understood backwards; but... it must be lived forward' with or without you in the near future. Last but not least, not to forget my family for their support during this demanding period.

# *Erklärung*

Hiermit erkläre ich an Eides statt, daß ich die vorliegende Dissertation selbständig verfaßt, keine anderen als die angegebenen Hilfsmittel verwendet und noch keinen Promotionsversuch unternommen habe.

Darmstadt, den 28. Nov 2005,

gez. Georgios Karolos Tsiledakis.

---

Unterschrift